1965

Antiferromagnetism in dilute chromium alloys

Alan LaMar Trego
Iowa State University

ANTIFERROMAGNETISM IN DILUTE CHROMIUM ALLOYS

by

Alan LaMar Trego

A Dissertation Submitted to the

Graduate Faculty in Partial Fulfillment of

The Requirements for the Degree of

DOCTOR OF PHILOSOPHY

Major Subject: Physics

Approved:

Signature was redacted for privacy.

In Charge of Major Work

Signature was redacted for privacy.

Head of Major Department

Signature was redacted for privacy.

Dean of Graduate College

Iowa State University
Of Science and Technology
Ames, Iowa

1965

TABLE OF CONTENTS

INTRODUCTION

During the past few years there have been a considerable number of investigations directed towards understanding the nature of the antiferromagnetic state in chromium. The interest in chromium arises because the magnetic transition differs from the usual one in which a system of disordered localized moments becomes ordered below some transition temperature. Furthermore, the magnetic ordering is not the ordinary antiferromagnetic structure in which neighboring localized spins have the same magnitude but are arranged antiparallel.

Early studies using impure, polycrystalline samples of chromium did not indicate clearly whether or not anomalies in the physical properties corresponded to a transition from a paramagnetic to an antiferromagnetic state. Recent careful measurements of the transport properties (1, 20, 45), the specific heat (7), the magnetic susceptibility (16), and the elastic properties (8, 41) of pure chromium together with extensive neutron diffraction measurements (3, 16, 46, 48) have shown that pure, strain free, chromium is indeed antiferromagnetic with a Néel temperature of about $312^{\circ}K$.

Attempts have been made to explain this type of anti-

ferromagnetic behavior in terms of static spin density waves (43, 50). For completely free electrons a spin density wave is a state which has a fractional spin polarization at every point in space. The direction of the polarization may vary from point to point as in the case of a helical spin density wave. If the spin density wave is associated with electrons which have some degree of localization, then the spin polarization function contains a factor which reflects the degree of localization. In general the periodicity of the spin density wave is different from the lattice periodicity. The basic idea of the theory of spin density waves is that under certain conditions the electron system in the paramagnetic state is unstable with respect to formation of a spin density wave. Thus a study of the magnetic properties of such systems with slightly different electronic structures should give additional insight into the nature of the antiferromagnetic state, as well as providing information with which to test the existing theories.

A study of the properties of dilute alloys of chromium appears to be a fruitful way to make such an investigation. This type of a study is appealing because the Néel temperature is altered considerably by the addition of relatively

small amounts of vanadium, manganese, and rhenium, while the alloys retain the b.c.c. structure of pure chromium and the lattice constants remain practically unchanged. With these alloys, then, the Fermi level is changed while the Brillouin zone boundaries remain practically the same.

Because the thermoelectric power (36) and electrical resistivity (1) of pure Cr single crystals show particularly striking anomalies, it appeared that a measurement of these properties for different alloys might provide information with which to test the theories. The difficulty associated with such a study in the past has been a lack of suitable samples. Previous investigations have shown that the magnitude of anomalies in both the thermoelectric power and the electrical resistivity is very sensitive to such factors as the grain size and strain of polycrystalline samples (18, 37). Therefore single crystals are necessary if one is to make a comparison of the magnitude of the anomalies as a function of alloy concentration.

As a result of efforts to purify chromium and vanadium and to investigate the effect of alloying upon the ductility of chromium, large single crystals of chromium alloys have become available at the Ames Laboratory (14). Measurements

of the transport properties of such chromium alloy crystals were therefore undertaken. Also, in cooperation with H. Bjerrum Møller, neutron diffraction measurements were made on these chromium alloy single crystals in order to make a more direct determination of their magnetic structure.

During the course of this investigation anisotropic behavior of the magnetic structure of chromium was reported (40, 54). This behavior arises when a single crystal of pure chromium is cooled through its Néel temperature either in a magnetic field or under strain. This effect should cause an anisotropy in the thermoelectric power and electrical resistivity. A study was therefore made of the electrical resistivity of field cooled specimens of chromium as a part of the effort to understand the antiferromagnetism of chromium.

CHROMIUM

Magnetic Structure

The Néel temperature of pure, strain free chromium is about 312°K. An early neutron diffraction investigation by Shull and Wilkinson (49) showed that chromium is antiferromagnetic. However, their measurements, which were made on a powdered sample, indicated a Néel temperature of about 450°K whereas anomalies in other physical properties (1, 19, 53) occurred near 312°K. Corliss et al. (17) first made neutron diffraction measurements on a pure single crystal of chromium. The Néel temperature indicated by their measurements was about 312°K, in agreement with the results observed for other physical properties. The higher ordering temperature observed in the powdered sample is probably related in some way to strains in the sample (37). Corliss et al. (17) also observed a long range modulation of the antiferromagnetic moment distribution. This conclusion was based on the fact that the diffraction peak which occurs near the (100) point in reciprocal space was found to be split into several satellite peaks. At room temperature they found satellite peaks at the $(1 \pm \delta, 0, 0)$, $(1, \pm \delta, 0)$, and $(1, 0, \pm \delta)$,

points in reciprocal space where δ is approximately 1/28. These satellites were also observed by Bacon (3). Initially the presence of the satellites was explained by assuming that chromium had an antiferromagnetic structure in which the body center spin was arranged antiparallel to the corner spin, however every 14 unit cells the structure underwent a 180° spin reversal. A later neutron diffraction investigation by Shirane and Takei (47), however, showed that the secondary satellites which were expected from the antiphase structure proposed by Corliss et al. (17) did not occur. Thus the antiferromagnetic structure is one in which the magnetic moments are modulated sinusoidally along the cube axes in the form of a wave.

Bykov et al. (13) and Bacon (3) observed that the satellite peaks at $(1 \pm \delta, 0, 0)$ disappeared below about 121°K. This is interpreted as resulting from a "spin flip" transition in which the magnetization waves change from the transverse type above 121°K to the longitudinal type below 121°K. This conclusion is based on the fact that there is no magnetic scattering from a magnetic moment which is parallel to the scattering vector. Hence, one expects that the $(1 \pm \delta, 0,0)$ satellites will disappear while the other satellite

peaks will, in fact, be enhanced for a change from transverse to longitudinal type magnetization waves. This behavior was observed by Bacon (3). From the neutron diffraction investigations, then, the following magnetic structure has been deduced. Below about 121°K the moment direction is parallel to one of the cube axis and the magnitude of the moment is modulated sinusoidally along the same axis with a repeat distance ($1/\delta$) of approximately 21 lattice constants.

Above 121°K the longitudinal arrangement becomes a transverse one and the period increases with increasing temperature up to approximately 27 lattice constants near the Néel temperature. The amplitude of the moment oscillation extrapolated to 0°K is about 0.58 μ_B (56). An alternative explanation of the neutron diffraction data in the temperature range 121°K to 312°K is that the spin arrangement is helical.

The above description, of course, would lead to tetragonal symmetry for chromium which is not observed. There are two models which are consistent with the neutron diffraction data and which can account for the cubic symmetry.

I. The magnetic structure of chromium consists of small magnetic domains each having a single linear mag-

netization wave in the [100] direction. The crystal consists of a statistical distribution of domains with wave vectors along [100], [010], and [001] directions. Each domain in this case has tetragonal symmetry.

II. Each magnetic domain consists of 3 linear magnetization waves respectively along the [100], [010], and [001] directions. Each domain in this case has cubic symmetry and it is possible for a good crystal to consist of one domain.

The results of an X-ray investigation by Weiss (55) favors the latter type of structure.

Wilkinson et al. (56) attempted to observe diffuse neutron scattering above the Néel temperature with a pure isotopic sample of Cr^{52}. Their results indicated that localized moments do not exist above the Néel temperature. The observation of a nuclear magnetic resonance above the Néel temperature in chromium by Barnes and Graham (5) also confirms the absence of localized moments. Further support for this idea is also obtained from the absence of a large anomaly in the specific heat (7) which accompanies the magnetic transition. The entropy change actually found is

netization wave in the [100] direction. The crystal consists of a statistical distribution of domains with wave vectors along [100], [010], and [001] directions. Each domain in this case has tetragonal symmetry.

II. Each magnetic domain consists of 3 linear magnetization waves respectively along the [100], [010], and [001] directions. Each domain in this case has cubic symmetry and it is possible for a good crystal to consist of one domain.

The results of an X-ray investigation by Weiss (55) favors the latter type of structure.

Wilkinson et al. (56) attempted to observe diffuse neutron scattering above the Néel temperature with a pure isotopic sample of Cr^{52}. Their results indicated that localized moments do not exist above the Néel temperature. The observation of a nuclear magnetic resonance above the Néel temperature in chromium by Barnes and Graham (5) also confirms the absence of localized moments. Further support for this idea is also obtained from the absence of a large anomaly in the specific heat (7) which accompanies the magnetic transition. The entropy change actually found is

about 0.0044 cal/deg whereas one would expect to see an entropy change of approximately (1/2)R ln2 = 0.7 cal/deg if a system of disordered localized moments became ordered. Thus, it appears that any moments which exist in the antiferromagnetic state must be induced during the ordering process. A study of the critical scattering of neutrons by Møller et al. (39) indicated, however, that a considerable amount of short range order persists in chromium to an unusually high temperature above the Néel temperature.

There have been several attempts to interpret the magnetic properties of chromium. Lidiard (31) first suggested that the antiferromagnetism of chromium is associated with the conduction electrons and showed that the small anomalies in the specific heat and magnetic susceptibility can be understood in this way. Overhauser (43) proposed a theory of spin density waves in which he tried to show that a state of a free electron gas with unbalanced up and down spins in the form of a wave in space should have a lower energy than that of the paramagnetic state. The spin polarization for a longitudinally polarized wave can be represented by

$$\vec{P} = P_o(\vec{x}\cos Qx + \vec{y}\cos Qy + \vec{z}\cos Qz) \quad . \qquad (1)$$

This type of polarization could be used to describe the

magnetic structure of chromium below 121°K. The true spin polarization would, of course, contain other Fourier components due to modulation of the three fundamental waves by the periodicity of the lattice. The effective exchange interaction between a moving electron of spin $\vec{s}$ and the spin density wave would be

$$H = - G (Q) \vec{s} \cdot \vec{P} \qquad (2)$$

where G (Q) is an appropriate exchange constant. Such an interaction can be considered as a perturbation on the free electron gas in the same manner as the periodic lattice potential is taken into account in the nearly free electron approximation. In the case under consideration an energy gap appears in the conduction electron dispersion curves at points in reciprocal space defined by

$$\vec{k}^2 = (\vec{k} + \vec{Q})^2 \qquad (3)$$

with the magnitude of the energy gap proportional to the amplitude of the spin density wave. As will be seen later, the appearance of such energy gaps can cause anomalies in the transport properties. By assuming that the ground state is a spin density wave state, Overhauser could qualitatively

account for some of the unusual properties of chromium.

From the mathematical similarities of his theory to the BCS theory of superconductivity (6), Overhauser deduced that the temperature dependence of the amplitude P_o of a spin density wave should be very similar to the temperature dependence of that of the superconducting energy gap. This is in contrast to the usual case where the temperature dependence of the magnitude of the magnetic moment follows a Brillouin curve. Using relative values of P_o obtained from the neutron diffraction results of Shirane and Takei (47), he was able to obtain a reasonably good fit to the theoretical curve obtained from BCS theory. From this he proposed that the magnitude of the energy gap for Cr should be about $3.5\ kT_N = 0.1eV$. On the basis of Overhauser's theory, then, the magnitude of the energy gaps should be proportional to T_N for materials having a SDW ground state.

Overhauser made his calculation within the framework of the Hartree-Fock approximation and used the true Coulomb force for the electron-electron interaction. This is a point of difficulty because the Coulomb interaction is screened by plasma oscillations. He found that the paramagnetic state of an electron gas is never the HF ground state but that the

paramagnetic state is always unstable with respect to formation of a static spin density wave of wave vector $Q = 2k_f$, the diameter of the Fermi sphere. Thus one expects to find spin density waves whose period is incommensurate with the lattice. His proof is independent of the density of the electron gas so it is difficult to see why more materials do not have a SDW ground state if the theory is correct.

Overhauser's theory is based on a free electron gas which is a poor approximation to the electronic structure of chromium. A calculation of the band structure of chromium by Asdente and Friedel (2) with the approximation of tight binding with d orbitals only and a consideration by Lomer (32) of a modification of their results when the 4s orbital is included indicates that electrons near the Fermi surface have principally d- character. Theories by Yosida (58) and by Tachiki and Nagamiya (50) treated the instability of the electron system by considering band electrons. Yosida (58) has suggested that the important difference between the free electron gas and the band electrons is that Umklapp-processes exist for the band electrons because of a periodic arrangement of the atoms in space. These Umklapp processes can enhance the stability of sinusoidal or helical spin density

waves. The theory of Tachiki and Nagamiya has shown that an electron system in a narrow band may have a state with a helical or sinusoidal spin density wave as a more stable state than the paramagnetic or ferromagnetic state.

Tachiki and Nagamiya also use the Hartree-Fock scheme and consider the band electrons to be characterized by Bloch functions

$$\phi(r,k) = \sqrt{1/N} \sum_{R} w(r,R) \exp (i\vec{k} \cdot \vec{R}) \qquad (4)$$

where w(r,R) is the Wannier function associated with the lattice site R and is assumed to be well localized. Because of the localization of the Wannier function, the Coulomb exchange interactions between electrons can be taken into account by including only those integrals

$$\int w(1,R_1)\ w^*(2,R_2)\ 1/r_{12}\ w(1,R_3)\ w(2,R_4)\ dV_1 dV_2 \qquad (5)$$

for which $R_1 = R_2 = R_3 = R_4$, i.e., we retain only the intra-atomic Coulomb integral and denote it by U. The value of this integral is reduced to some effective value, U_{eff}, because of electron correlations and has a value of a few eV.

Assuming, for example, a helical spin ordering the spin direction of each atom varies as $(\cos \vec{q}\cdot\vec{R}_n, \sin \vec{q}\cdot\vec{R}_n, 0)$ with

atom position R_n. The interaction between a moving electron with spin $\vec{s}$ and the crystal is then

$$-2 \sum_n g(\vec{r} - \vec{R}_n) \, (s_x \cos \vec{q}\cdot\vec{R}_n + s_y \sin \vec{q}\cdot\vec{R}_n) \qquad (6)$$

where g is the spin density function associated with each atom and is assumed to be well localized. Again because the Wannier functions are localized only those integrals

$$\bar{g} = \int w^*(\vec{r} - \vec{R}_1) \, g(\vec{r} - \vec{R}_m) \, w \, (\vec{r} - \vec{R}_n) \, dV \qquad (7)$$

for which $R_1 = R_m = R_n$ are included. By minimizing the total energy with respect to $\bar{g}$, Tachiki and Nagamiya obtain the self consistent relation

$$\bar{g}^2/U = 1/2N \, [\Sigma^+ \mp \bar{g}^2/(\bar{g}^2 + x^2)^{1/2} + \Sigma^- \mp \bar{g}^2/(\bar{g}^2 + x'^2)^{1/2}] \qquad (8)$$

where

$$x = 1/2 \, [\epsilon(\vec{k} + \vec{q} + \vec{K}) - \epsilon(\vec{k})] \qquad (9)$$

$$x' = 1/2 \, [\epsilon(\vec{k} - \vec{q} - \vec{K}') - \epsilon(\vec{k})] \qquad (10)$$

and $\vec{K}$ and $\vec{K}'$ are reciprocal lattice vectors. The two sums have the same value.

$\bar{g} = 0$ is the solution which gives the paramagnetic state. To find other solutions $\bar{g}2$ is eliminated from both

sides of the equation. The right hand side is a decreasing function of $\bar{g}2$ with q as a parameter. If the value of the function at $\bar{g} = 0$ is higher than 1/U then one can obtain a non-vanishing $\bar{g}$ value which satisfies (8) and this corresponds to the self-consistently created helical spin arrangement. The q value is determined to give the lowest energy.

The actual calculation of the sums, which are equal, is very complicated because the Fermi surface is not spherical. Tachiki and Nagamiya have carried out the sums, by neglecting $\bar{g}2$ in the denominators and by assuming a spherical Fermi surface, as a function of q for different radii of the Fermi surface. Their results are shown in Figure 1. For $k_f = \pi/a$ (curve 1) the curve has a maximum at $q = 2\pi/a$. This means that antiferromagnetic ordering would set in when U just exceeds the value corresponding to this maximum. When k_f is 1.5% smaller than π/a, a maximum (curve 2) occurs for $q = 0.96(2\pi/a)$. Hence, if U exceeds the critical value corresponding to this maximum, we would have an antiferromagnetic helix of repeat distance 22a. Curve 3 is for a k_f which is 3% smaller than π/a and the corresponding period is 14a. Continuing to decrease k_f causes the maximum of the curve to decrease until finally the highest point on the curve is at $q = 0$. In this case ferromagnetism could occur

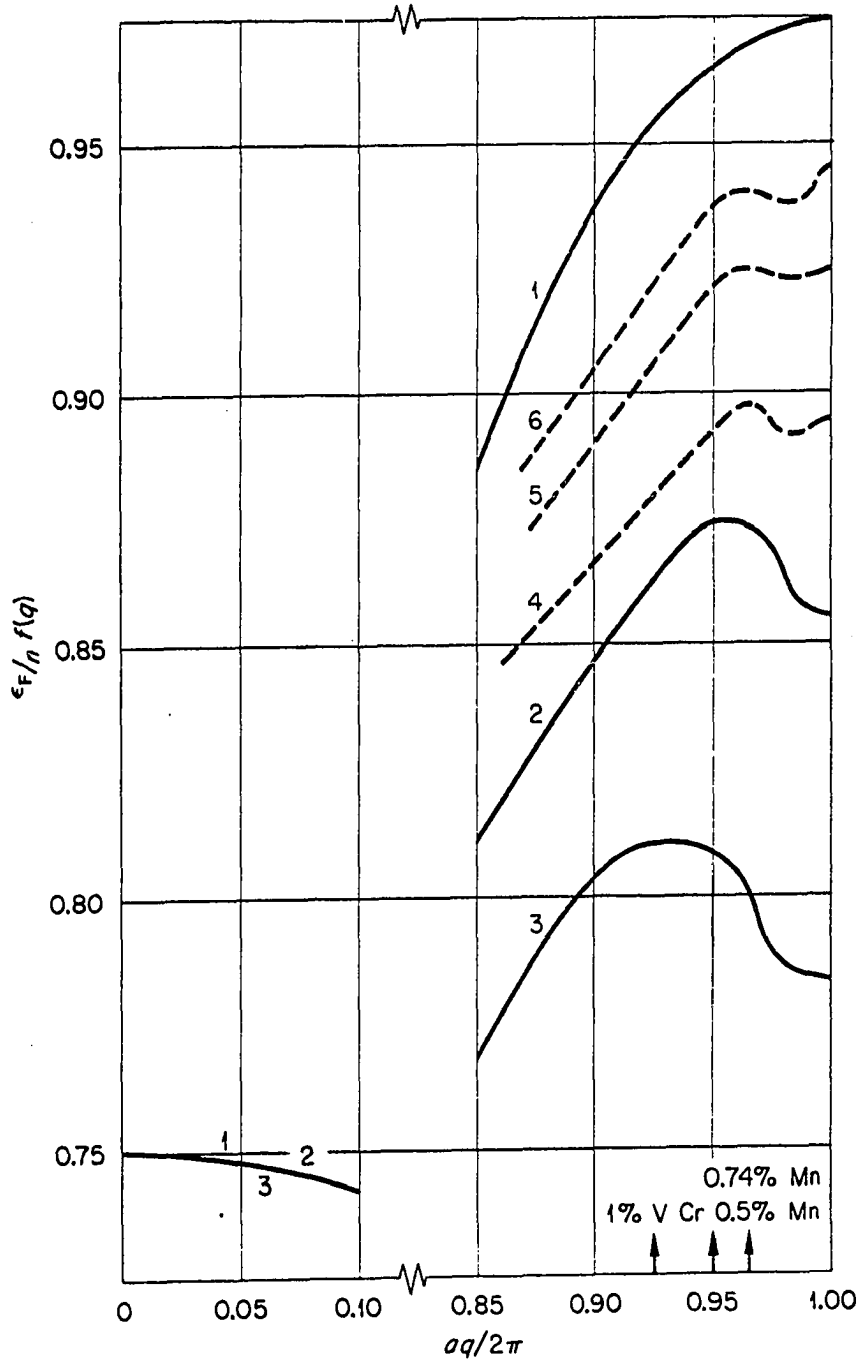

Figure 1. Curves of (ϵ_f/n) f (q) versus q ((f/q) = $(1/N)\Sigma^{+}(1/x)$ and ϵ_f and n are the Fermi energy and number of electrons per atom)

for certain U values which exceed some critical value. When k_f is greater than π/a the maximum occurs at $q = 2\pi/a$ and we may have a simple antiferromagnetic structure for appropriate values of U. This theory, therefore, predicts that the kind of antiferromagnetism which occurs in chromium can occur for only a limited range of electron concentration. Above a certain electron concentration the simple antiferromagnetic structure will appear. As the electron concentration is decreased, the period of the magnetization waves will decrease. By alloying chromium with small amounts of vanadium, rhenium, and manganese changes in electron concentration can be realized and the predictions of the theory tested.

Static and Transport Properties

There have been extensive investigations of the static and transport properties of pure chromium. A careful measurement of the specific heat by Beaumont et al. (7) revealed a small but distinct anomaly at the Néel temperature. As mentioned in the previous section, the absence of a large anomaly indicates that localized moments are absent above the ordering temperature.

Interpretation of magnetic susceptibility measurements on Cr is difficult because the compound Cr_2O_3, which is always

present as an impurity, has a Néel temperature of 40°C. A recent study of the magnetic susceptibility by Collings et al. (16) on samples of various purity indicates that the maximum in the susceptibility cannot be accounted for by the presence of Cr_2O_3 and, therefore, must be related to the electronic structure of chromium itself.

Studies of the elastic properties (8, 41) show anomalies at 40°C in the Young's modulus, internal friction, and thermal expansivity.

The temperature dependence of the Hall coefficient was measured by de Vries and Rathenau (53). They found a large, positive value in both the paramagnetic and antiferromagnetic region which corresponds to a small number of holes as the dominant charge carriers. A straightforward analysis of charge carrier concentration is not possible because chromium has unfilled s and d bands. At the Néel temperature de Vries and Rathenau found a change of slope in the curve of R_H versus T.

There have been a considerable number of measurements of both the electrical resistivity and the thermoelectric power of pure chromium.

A number of investigators have established the existence of a minimum in the resistivity versus temperature curve for

pure chromium in the temperature region 12-40°C (1, 20, 37). The magnitude and location of the anomaly found by the different investigators varied considerably. De Morton (41) found that cold work eliminates this minimum. This result was verified by Marcinkowski and Lipsitt (37) who studied both a plastically deformed sample and a recrystallized sample. They concluded that the discrepancies in the position of the Néel temperature and in the magnitude of the anomaly was due to a lack of proper annealing of the samples. A study of the resistivity of a single crystal of pure chromium by Arajs et al. (1) revealed also that the thermal history of the sample may be important.

Overhauser (43) has accounted for the presence of this minimum on the basis of his spin density wave model. As a result of the spin density wave exchange potential, the Fermi surface is truncated by energy gaps. The effect of the distortion of the Fermi surface on the resistivity is to cause an increase of resistivity with decreasing temperature immediately below the Néel temperature. This effect is discussed in considerably more detail in a following section.

An anomaly in the thermoelectric power of polycrystalline samples near 40°C has been observed by several workers (18, 20). A thorough study by Edwards (18) using samples of

different grain size, of different hardness, and with different amounts of interstitial impurities showed that the magnitude of the anomaly is highly dependent upon grain size and hardness but is essentially independent of interstitial impurities. Thus, it would be highly desirable to have well annealed single crystals to study this property of chromium. The thermoelectric power of a single crystal of Cr was measured as a function of temperature by Mackintosh and Sill (36). They found a positive thermoelectric power over the whole range studied. Just below the Néel temperature a large hump was observed which they interpreted in terms of the Overhauser spin density wave model. The large increase observed is primarily due to the energy gaps in the Fermi surface together with a rapid variation of the magnetic disorder scattering (see a following section).

Chromium Alloys

The temperature at which the anomaly in chromium occurs is very sensitive to the addition of metallic impurities. De Vries (52) investigated the effect on the electrical resistance and Hall coefficient of alloying chromium with about one atomic per cent of vanadium, manganese, iron, cobalt and nickel. He found that vanadium caused the transi-

tion temperature to shift down to 240°K and that one per cent manganese caused the transition temperature to shift up to 190°C. He concluded that the transitions observed were of an electronic nature but could not deduce whether or not they corresponded to Néel temperatures.

The electrical resistivities of polycrystalline chromium-vanadium alloys (0.5% V, 1.5% V, 2.5% V, and 5% V) were measured by Taylor (51). He found that the anomaly had shifted below 77°K for the 5% V sample and that the form of the anomaly of the 2.5% V sample was considerable different from that for the 0.5% V and 1.5% V samples. Taylor's results for the transition temperature as a function of atomic per cent V are shown in Figure 2.

The Néel temperatures of Cr-V alloys have been accurately determined by Barnes and Graham (5). They observed the vanishing of the V^{51} and Cr^{53} nuclear magnetic resonances at the onset of magnetic ordering. The curve obtained by them for Néel temperature as a function of electrons per atom is shown in Figure 24.

The Néel temperatures of chromium-manganese alloys containing from 7.0 to 55.3 atomic per cent manganese have been determined by Hamaguchi and Kunitomi (25) and are shown in Figure 2. They made neutron diffraction, electrical resis-

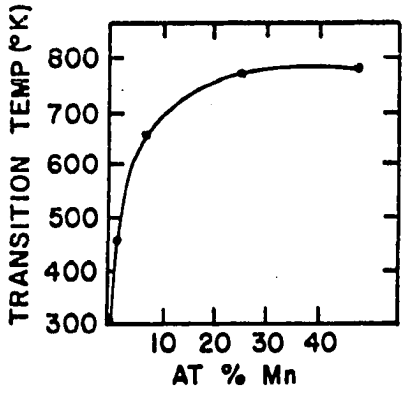

(a) Cr-MN ALLOYS

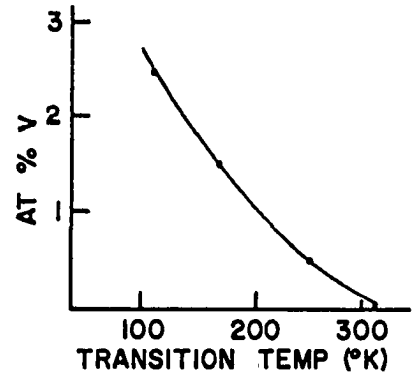

(c) Cr-V ALLOYS

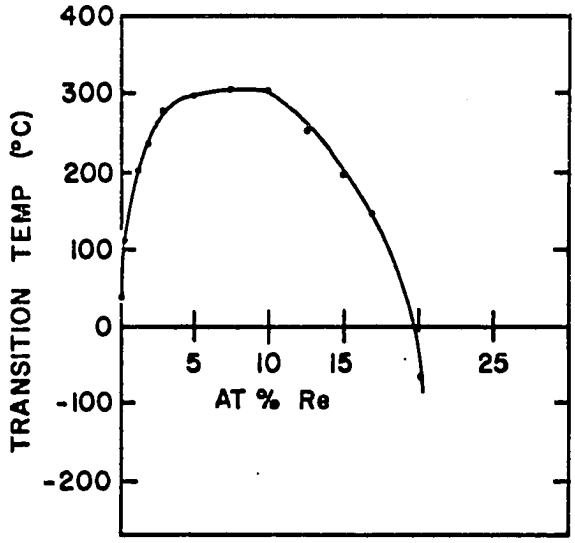

(b) Cr-Re ALLOYS

Figure 2. Transition temperature versus alloy concentration (a. Cr - Mn alloys; b. Cr - Re alloys; c. Cr - V alloys)

tivity, and magnetic susceptibility measurements of polycrystalline samples. They concluded that the alloys are antiferromagnetic but are disordered atomically. The observed magnetic moment and Néel temperature of the alloys initially increased rapidly with increasing manganese concentration and approached saturation at about 30 atomic per cent Mn. They studied the temperature dependence of the magnetic moment of a 25.3% Mn alloy as a function of temperature. Their results show that the experimental points lie on a curve similar to that predicted by BCS theory (6) for the temperature dependence of the superconducting energy gap rather than on a Brillouin function curve. This point is in good agreement with the prediction of Overhauser's theory (43). Their experimental resolution was insufficient to resolve any possible satellite peaks.

In a recent experiment by Hamaguchi et al. (26) the magnetic properties of chromium alloys with small amounts of manganese (0.5%, 0.74%, 2.1%) and vanadium (1.0%, 1.9%) were investigated by neutron diffraction. In this case, the experimental resolution was adequate to detect satellite peaks. They found satellites for the 0.5% Mn and 0.74% Mn sample but did not observe satellites at any temperature between 5°K and 400°K for the 2.1% Mn sample.

They concluded that the modulated magnetic structure of chromium near room temperature is made less stable by the addition of small amounts of manganese and that a simple antiferromagnetic structure phase begins to appear. The stability of the simple antiferromagnetic phase increases with increasing Mn concentration. The sinusoidally modulated structure is still stable at low temperatures for Mn concentrations less than 0.5%. The low temperature, longitudinally polarized, phase of chromium is less stable than the high temperature phase and disappears in the 2.1% Mn alloy.

For the 1.9% V alloy they observed a single phase of transverse polarization existing from T_n to 4.2°K. At 77°K they found a periodicity of 13.2 unit cells.

The magnetic susceptibilities and electrical resistivities of polycrystalline chromium-rhenium alloys have been studied by Booth (9). He finds that the temperature at which anomalies occur varies rapidly with rhenium concentration, reaching a maximum of about 580°K for a composition of 5 atomic per cent rhenium, remaining approximately constant until 10 atomic per cent rhenium is reached and then decreasing rapidly to 170°K at about 20 atomic per cent rhenium. He observed anomalies in the resistivities similar to that

found in pure chromium but of differing magnitudes. His curve of T_n versus atomic per cent Re is shown in Figure 2.

Butylenko and Gridnyev (12) have studied the effect on the position of the Néel point and on the magnitude of the anomalies of alloying chromium with elements of the third long period from Lu to Os, as well as Ru, by measuring the electrical resistivity, the thermoelectric voltage and the thermal expansion. They found that Lu, Hf, Ta and W lowered the Néel temperature while Re, Os and Ru raised the Néel temperature. They were unable to correlate the antiferromagnetic properties and the plasticity of chromium and its alloys.

TRANSPORT PROPERTIES

Electrical Resistivity

Accounts of the theory of the electrical resistivity, ρ, for nonmagnetic metals have been given by Ziman (59), Wilson (57), and Mott and Jones (42). There is a region at low temperatures where the electrical resistance is temperature independent and depends on scattering from lattice defects or impurities. This is followed by a region for which ρ increases as T^5 due to phonon scattering. Finally at higher temperatures, above about one-fifth of Θ_D, the phonon scattering gives a resistance proportional to T.

If the scattering can be described by a relaxation time, then the electrical conductivity can be calculated from

$$\sigma_{ij} = (e^2\tau/4\pi^3\hbar)\int v_i dS_j \qquad (11)$$

where e is the electronic charge, $\hbar$ is Planck's constant, τ is the relaxation time, v_i is a component of the electron's velocity at the Fermi surface, and S_j is the jth component of the Fermi surface vector.

An account of the electrical resistivity of dilute alloys has been given by Mott and Jones (42). The tempera-

ture dependence remains of the same form as that for a pure metal. Mathiessen's rule states that the resistivity of a dilute alloy can be represented by

$$\rho = \rho_L(T) + \rho_r(x) \qquad (12a)$$

where $\rho_L(T)$ is a function of temperature and represents the electrical resistivity of an ideal metal. $\rho_r(x)$ is temperature independent but depends on the type and amount of the impurity. According to Nordheim's rule the residual resistivity, $\rho_r(x)$, of a binary alloy containing a mole fraction x of element A and (1 - x) of element is given by

$$\rho_r \sim x(1-x). \qquad (12b)$$

The effect which is of primary interest to this study is the influence of magnetic moments and magnetic ordering on the electrical conductivity. The presence of magnetic moments in a magnetically ordered state can cause changes in both the relaxation time, τ, and in form of the Fermi surface. Kasuya (29) and de Gennes and Friedel (22) have considered the effect of magnetic scattering on the relaxation time for ferromagnetic and antiferromagnetic materials. They assume that the magnetic scattering is additive to the

impurity and phonon scattering, thus

$$1/\tau = 1/\tau_{imp} + 1/\tau_{ph} + 1/\tau_{m}. \qquad (13)$$

At temperatures far above the ordering temperature the moments are completely disordered and τ_m is a constant. At temperatures just above the ordering temperature short range order is present and τ_m decreases slowly with decreasing temperature. Below the ordering temperature τ_m increases with decreasing temperature as the order of the system becomes more complete and finally τ_m becomes infinite when the system is completely ordered.

Thus far only the effect on the relaxation time has been considered. If the magnetic moments are ordered then the value of the integral may be changed. This can happen when the periodicity of the magnetic order is different from the periodicity of the lattice. New Brillouin zones of magnetic origin will be introduced which may intersect the Fermi surface and cause energy gaps to appear. Miwa (38) and Elliott and Wedgwood (19) have considered this problem on a free electron basis for a gap of width Δ_i in the ith direction and find that the resistivity is given by

$$\rho_i = \rho_r + \rho_L(T) + \rho_m(T)/(1-\alpha_i) \qquad (14)$$

where $\rho_m(T)$ is the contribution of the magnetic disorder scattering. For the free electron model α_i is given by

$$\alpha_i = (3\pi/4)(\ell/k_f)(\Delta_i/E_f) \qquad (15)$$

for the case where the new zone boundary cuts the Fermi surface into two parts, and by

$$\alpha_i = 1 - (\ell/k_f)^3 + (3\pi/8)(\ell/k_f)(\Delta_i/E_f) \qquad (16)$$

for the case where the Fermi surface touches the new boundary but has no second portion beyond it. k_f is the radius of the Fermi sphere, E_f is the Fermi energy and ℓ is the perpendicular distance in k space from the origin to the superzone boundary. For the directions perpendicular to i the effect on the resistivity is of second order in α_i and can usually be neglected. This theory was used to account for the humps appearing in the electrical resistivities of dysprosium and holmium just below their Néel temperatures. The theory also accounts for the fact that the hump occurs only for the resistance along the [0001] direction and does not occur in the basal plane resistance.

Thermoelectric Power

Experimentally it is found that an electric field exists in a conductor which is subject to a thermal gradient, thus

$$\vec{E} = S \vec{\nabla} T \tag{17}$$

where $\vec{E}$ is the electric field, T is the absolute temperature, and the coefficient S is called the thermoelectric power. This effect was discovered in 1821 by Seebeck. In the general case the thermoelectric power is a second rank tensor.

A closely related effect was discovered by Peltier in 1834. He found that if two conductors are kept at constant temperature and a dc current, I, passes through the circuit then heat, in addition to the joule heat, is produced or absorbed at the junctions at a rate

$$\dot{Q} = \pi_{12} I. \tag{18}$$

The coefficient π_{12} is called the Peltier coefficient. This is a reversible effect since it depends linearly on the current I.

Another related effect was predicted by Thomson in 1854 and was discovered in 1856. For this effect it is found that

if a current, I, passes through a conductor in which there is a temperature difference, ΔT, an amount of heat

$$\dot{Q} = \mu I \, \Delta T \tag{19}$$

is absorbed or generated per second in addition to the Joule heat. The coefficient μ is called the Thomson coefficient. Again this effect is reversible since it depends linearly on the current, I, in contrast with the irreversible Joule heating.

These thermoelectric effects can be fit quite naturally into a scheme involving the usual transport coefficients, σ the electrical conductivity and κ, the thermal conductivity (59, p. 270).

Of fundamental importance to the study of the thermoelectric effects is the existence of the Kelvin relations. On the basis of irreversible thermodynamics, one can derive the following equations (59, p. 274)

$$\mu = T \, dS/dT \tag{20}$$

and

$$\pi = TS. \tag{21}$$

Thus, we can determine all of the thermoelectric proper-

ties of a material from a measurement of S. This is especially convenient because S can be measured relatively easily and quite accurately whereas μ and π must be measured by inherently difficult caliormetric methods.

Wilson (57), Ziman (59), and MacDonald (35) have given accounts of the theory of thermoelectric power. In terms of the electrical conductivity, S is given by

$$S = (\pi^2 k^2 T/3e)(\partial \ln \sigma(E)/\partial E)_{E_f} \qquad (22)$$

where k is Boltzmann's constant, T is the absolute temperature, e is the electronic charge, E is the energy of the electrons, and E_f is the actual Fermi energy. The expression means that one should calculate the electrical conductivity as a function of the hypothetical position, E, of the Fermi level, and then evaluate the derivative of $\ln \sigma(E)$ with respect to E at the actual Fermi energy E_f. In contrast to the electrical conductivity and thermal conductivity, S has an intrinsic sign since e appears to the first power.

The formula is valid for pure metals for temperatures much larger than the Debye temperature. The formula is valid for any functional relation between energy and wave number provided electron scattering can be adequately described by a

relaxation time. The formula is applicable to alloys even at low temperatures, provided that the resistivity from impurity scattering is much greater than the resistivity arising from phonon scattering.

For free electrons expression 1 is easily evaluated and we find $S_F = -2.45 \times 10^{-2}\ T/E_f$ microvolts per degree.

There are several mechanisms which can contribute to the total thermoelectric power of a metal. If the electrons are colliding solely with static defects in the lattice then the thermoelectric power is found to vary more or less linearly with temperature. For high temperatures, where the electron-phonon scattering can be described by a relaxation time, it is also found that the thermoelectric power should vary linearly with temperature. In both of these cases the effect of collisions is to restore the electron distribution to equilibrium and we have what is usually termed diffusion thermoelectric power.

However, if electron-phonon collisions are important and if the phonon distribution is not in equilibrium then this asymmetry will be transmitted to the electron distribution. The phonon distribution is not in equilibrium when a temperature gradient is present so that this effect will be of

importance to the thermoelectric power when the electron-phonon collisions become dominant. This occurs when T is much less than the Debye temperature and is found experimentally to reach a maximum at a temperature of about one-tenth to one-thirtieth of the Debye temperature. This is called phonon drag thermoelectric power and is found to increase as T^3 up to a maximum of about one-tenth of Θ_D and then to fall off as T^{-1} above this temperature. This effect can be either positive or negative depending upon whether normal or Umpklapp processes are dominant. The phonon drag contribution can cause a change of sign of S if it is larger than the diffusion contribution and has opposite sign.

In the case of diffusion thermoelectric power and phonon drag thermoelectric power it is found that the two effects are additive. In this case there are two separate sources of thermoelectricity. However, if there are two kinds of scatterers present then the total thermoelectric power is not simply the sum of the thermoelectric power that each one alone would give; but, instead, the total thermoelectric power is a weighted sum. The correct weighting factors are just the thermal resistivities, W_i, of each kind of scatterer, i.e.

$$S = \Sigma_i W_i Q_i / \Sigma_i W_i. \qquad (23)$$

For applications of this formula see Gold et al. (23), and Huebener (28). If we have a two band conductor then the total thermoelectric power is again a weighted sum of the contributions from each separate band. The correct weighting factors in this case are the electrical conductivities of each band, i.e.

$$S = \sum_i \sigma_i S_i / \sum_i \sigma_i. \qquad (24)$$

These formulas show that the thermoelectric power can be regarded as an intensive parameter whose magnitude depends on the relative concentrations of scatterers rather than on the absolute concentrations.

Thus, the effect on the thermoelectric power due to alloying may be quite different from the effect on the electrical resistivity.

If we use the general formula for the conductivity of a cubic metal

$$\sigma = e^2 \bar{\lambda} \Sigma / 12\pi^3 h, \qquad (25)$$

where $\bar{\lambda}$ is the mean free path and Σ is the Fermi surface area, in the expression for S we get

$$S = (\pi^2 k^2 T/3e)[\ \partial \ln(\bar{\lambda})/\partial E + \partial \ln(\Sigma)/\partial E\ ]_{E_f}. \qquad (26)$$

This formula shows that the thermoelectric power is extremely sensitive both to the energy dependence of the mechanisms which scatter electrons and to changes in the electronic structure. When studying an alloy system, however, one may get a combination of effects which may be difficult to separate.

The above discussion has been only for non-magnetic materials. Since the resistivity is affected by magnetic ordering one would also expect to see an effect on the thermoelectric power. Such effects have been observed, for instance, in the rare earth metals (48) and in pure Cr (36). Apart from these investigations very few studies have been made of the effect of magnetic ordering on the thermoelectric power either theoretically or experimentally.

Kasuya (30) has studied the effect of s - f interactions on the thermoelectric power of ferromagnets. He used the spin wave approximation for low temperatures and a molecular field approximation for temperatures just below the ordering temperature. Born (11) has measured the thermoelectric power of gadolinium and has compared his results with the predictions of Kasuya's theory. He found qualitative agree-

ment with the theory with the exception of a low temperature peak which can be ascribed to phonon drag. Kasuya found, however, that for an antiferromagnet there would be no extra contribution to the thermoelectric power.

Bailyn (4) and Gurevich and Nedlin (24) have considered the effect of spin-wave or magnon scattering on the thermoelectric power. Bailyn has found that a magnon drag contribution to the thermoelectric power is possible and is analogous to phonon drag. In general, he finds that it may be difficult to distinguish between phonon drag and magnon drag.

Mackintosh[1] has extended the considerations of Miwa (38) and Elliott and Wedgwood (19) to the case of the thermoelectric power. He uses the equation

$$S = (\pi^2 k^2 T/3e)(\partial \ln \sigma(E)/\partial E)_{E_f} \qquad (27)$$

as the starting point and stays within the free electron approximation. If the relaxation time varies as E^n then, for a magnetic superzone which cuts the Fermi surface into two parts, he finds

$$S = (\pi^2 k^2 T/2eE_f)[1/(1-\alpha_i) - n\tau/3\tau_m] \qquad (28)$$

---

[1]Mackintosh, A. R., Ames, Iowa. Thermoelectric power of magnetic materials. Private communication. 1964.

where α_i has the same meaning as in the electrical resistivity calculation. For details of this calculation see Sill (48, Appendix A).

EXPERIMENTAL TECHNIQUES

Materials and Sample Preparation

Single crystal ingots of chromium alloys with small amounts of vanadium, manganese and rhenium were generously provided by Dr. F. A. Schmidt of the Ames Laboratory. The crystals were grown by an arc-zone melting technique described by Carlson et al. (14). According to Hansen (27), chromium-vanadium and chromium-rhenium alloys have a complete range of solid solubility and crystallize in a bcc structure while chromium-manganese alloys form solid solutions for mixtures containing up to at least 25 atomic per cent manganese. The alloys used for this work were all within the region of solid solubility.

Iodide chromium, obtained from the Chromalloy Corporation, was used as the base metal throughout this investigation. Crystal bar vanadium was used to fabricate the chromium-vanadium alloys. The manganese used was obtained from the United Mineral and Chemical Corporation and the rhenium from Chase Brass Corporation. The nominal assays and impurity contents of the chromium, vanadium, manganese and rhenium are listed in Table 1.

Table 1. Nominal assay and impurity content of starting materials

The impurities are given in ppm and the nominal assays in weight per cent.

Chromium:	Nominal assay 99.98%
	N,21; C,57; O,10; H,1; Fe,40; Ca,1; Al,3; Mg,1; Cu,1; Mn,1; Mo,1; Si,20; Ni, 2; V,2.
Rhenium:	Nominal assay 99.99%
	Fe,10-20; Al,1; Ca,1; Cr,1; Mg,1; Cr,1; Si,1; C,40.
Manganese:	Nominal assay 99.99%
	Mg,5; Si,5; Cu,1.
Vanadium:	Nominal assay 99.2%
	O,168; H,7; N,6; Al,20; Ca,30; Cu,50; Fe,480; Mg,15; Mn,25; Ni,60; Si,40; Ti,90.

In the process of preparing single crystals the alloys were required to undergo several consolidation arc-melt and arc-zone melting operations. An analysis of a sample of pure Cr in the as-received, as arc-melted, and as arc-zone-melted condition is presented in Table 2. Only interstitial analyses are presented since it is not expected that metallic impurities will be introduced during the arc-melting operation.

Table 2. Interstitial impurity content of the base chromium as-received, as-arc-melted, and as arc-zone-melted

Interstitial impurity content, ppm			
Element	As-received	Arc-melted	Arc-zone-melted
N	21	40	30
O	10	22	16
C	57	79	72
H	1	1	1

The specimens were received in the form of single crystal ingots about 1/2 inch in diameter by 6 inches long. In some cases the ingot consisted of several large grains. Rectangular parallepipeds of about 2 mm square cross section by 15 mm long were cut from the ingots with a spark erosion cutter. The specimens were then electropolished in ortho-phosphoric acid and annealed to remove strains. The crystals were annealed at 1000°C for five hours and then were cooled at the rate of 40°C per hour.

The samples used for thermoelectric power and electrical resistivity measurements were of random orientation. Back reflection Laue X-ray pictures were taken of all samples to

ensure that they were indeed single crystals. The compositions of the alloys were determined by chemical analysis.

The pure chromium crystals which were used for the field cooling measurements were prepared with (100) type planes parallel to each face of the crystal. This was accomplished by mounting the crystal on a goniometer which had a permanently affixed rectangular base. By the use of back reflection Laue X-ray pictures the (100) planes of the crystal were aligned with the base. The whole assembly could then be transmitted to a spark cutter and the desired cuts made. The accuracy of the alignment was ± 2.0 degrees.

Apparatus and Method for Thermoelectric Power Measurements

In order to see how S is measured experimentally, consider the open circuit of Figure 3. We can write the open circuit potential difference as

$$\Delta V_{AX} = - \oint \vec{E} \cdot d\vec{r}. \tag{29}$$

But,

$$\vec{E} = S \vec{\nabla} T \tag{30}$$

so

$$\Delta V_{AX} = - \oint S \, T \cdot d\vec{r} = \int_{T_o}^{T + \Delta T} S_A dT + \int_{T + \Delta T}^{T} S_X dT + \int_{T}^{T_o} S_A dT \tag{31}$$

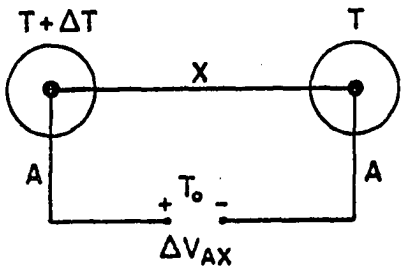

$$S_{AX} = \lim_{\Delta T \to 0} \frac{\Delta V_{AX}}{\Delta T} = \frac{dV_{AX}}{\Delta T} = S_A - S_X$$

(a) BASIC THERMOELECTRIC CIRCUIT

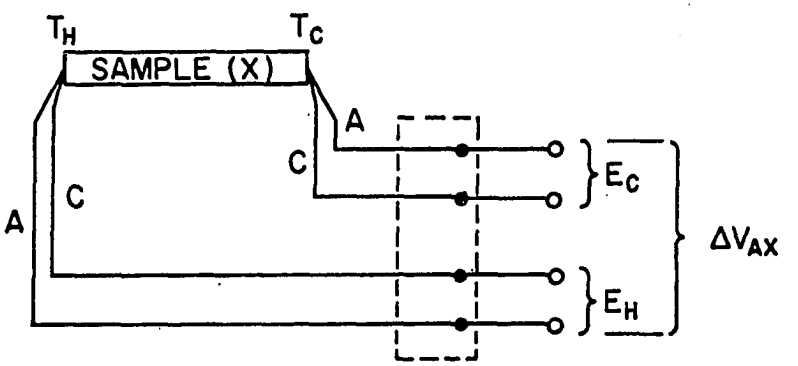

A = COPPER
C = CONSTANTAN OR Au + 0.03% Fe

$$S_{AX} = \frac{S_{AC}\ \Delta V_{AX}}{E_H - E_C}$$

(b) MEASURING CIRCUIT

Figure 3. Thermoelectric effect
(a) basic thermoelectric circuit
(b) measuring circuit

and therefore

$$\Delta V_{AX} = \int_{T}^{T + \Delta T} (S_A - S_X)dT = \int_{T}^{T + \Delta T} S_{AX}dT. \quad (32)$$

If $\Delta T/T << 1$ then

$$\Delta V_{AX} = (S_A - S_X)\ \Delta T + 0\ (\Delta T/T)^2. \quad (33)$$

Hence, only differences of S can be determined. One method of finding S for an individual metal is to use a superconductor as one of the conductors. This is useful because S is found to be very nearly zero for a superconductor. This can be used, however, only at low temperatures. A second method is to make use of one of the Kelvin relations. We can write

$$S\ (T) = S(T_o) + \int_{T_o}^{T} \mu/T\ dT. \quad (34)$$

Borelius et al. (10) have measured μ for lead and thus determined S. More recently Christian et al. (15) have improved the accuracy of S for lead at low temperatures by making measurements against a Nb_3 Sn superconductor.

A schematic diagram of the sample holder and heat leak chamber which was used for thermoelectric power measurements

is shown in Figure 4. The specimen was soldered between the two copper blocks with pure indium solder. A stainless steel soldering flux was required to make the solder stick to the samples. A temperature gradient of $2^{o}K$-$3^{o}K$ was provided by means of a small resistance heater glued to the upper copper block with G.E., type 7031 adhesive. The heater was constructed from 100 ohms of AWG #36, Formvar covered, manganin wire and was powered by a 12 volt Zener diode supply.

In order to provide continuously variable temperatures a heat leak chamber was used. The sample chamber was connected to the outer chamber by a 1" length of stainless steel tubing. The outer chamber was placed directly in a liquid helium, liquid nitrogen, dry ice and acetone slush, or ice bath depending upon the temperature range desired. A standard glass dewar system was used to hold the cryogenic materials. Any temperature above the bath could be obtained by evacuating the chamber and applying Joule heat to a resistance heater glued to the outside of the sample chamber. The heater was constructed of 100 ohms of AWG #32, Formvar covered, manganin wire.

The potential leads, which were AWG #38 copper wires, and the thermocouple wires were thermally anchored to the

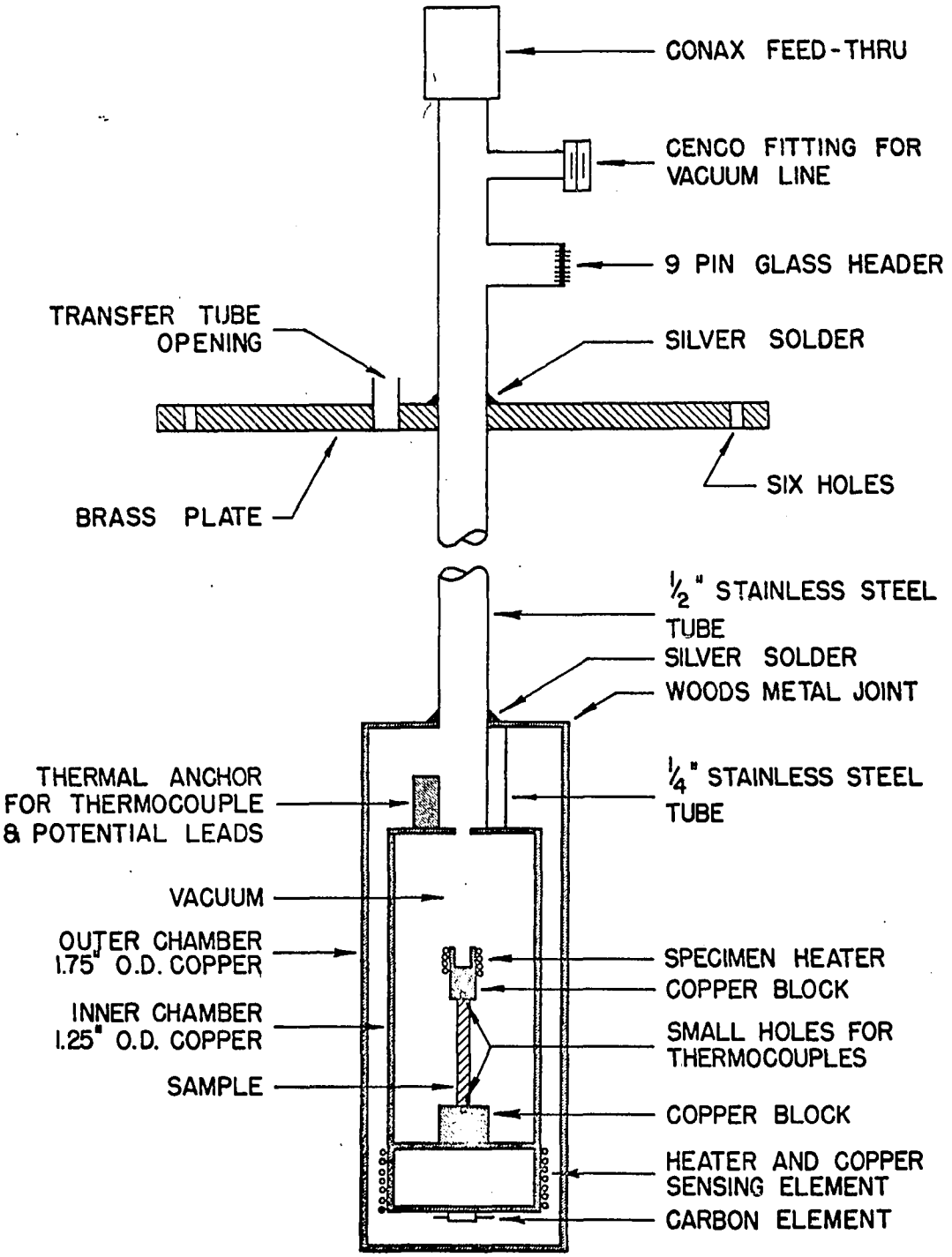

Figure 4. Sample holder for thermoelectric power measurements

sample chamber before making contact with the sample. Large temperature gradients in the wires in the vicinity of the junctions were thus eliminated. The thermocouple junctions could then come to equilibrium with the ends of the sample. No junctions were made in the potential leads and thermocouple wires except at the reference junction. This was accomplished by taking the leads out of the sample holder through a conax thermocouple gland. Sharp gradients were eliminated from the critical leads by using teflon tubing as insulation. Measurements were taken in a vacuum of about 1×10^{-5} torr.

All data were taken using a steady state heat flow method. This was accomplished by using an automatic temperature control system which was capable of reducing the temperature drift to less than $0.01^{\circ}K$ per minute. The temperature control system is shown in Figures 5, 6, and 7 and consisted of a temperature dependent resistance, a Wheatstone bridge, a d.c. amplifier, and a d.c. power supply. One arm of the bridge contained the sensing element and the other arm a variable Helipot resistor. Two sensing elements were used. A 100 ohm carbon resistor was used for the temperature range from $4.2^{\circ}K$ to $30^{\circ}K$. Both of these elements were placed in good thermal contact with both the heater and the sample

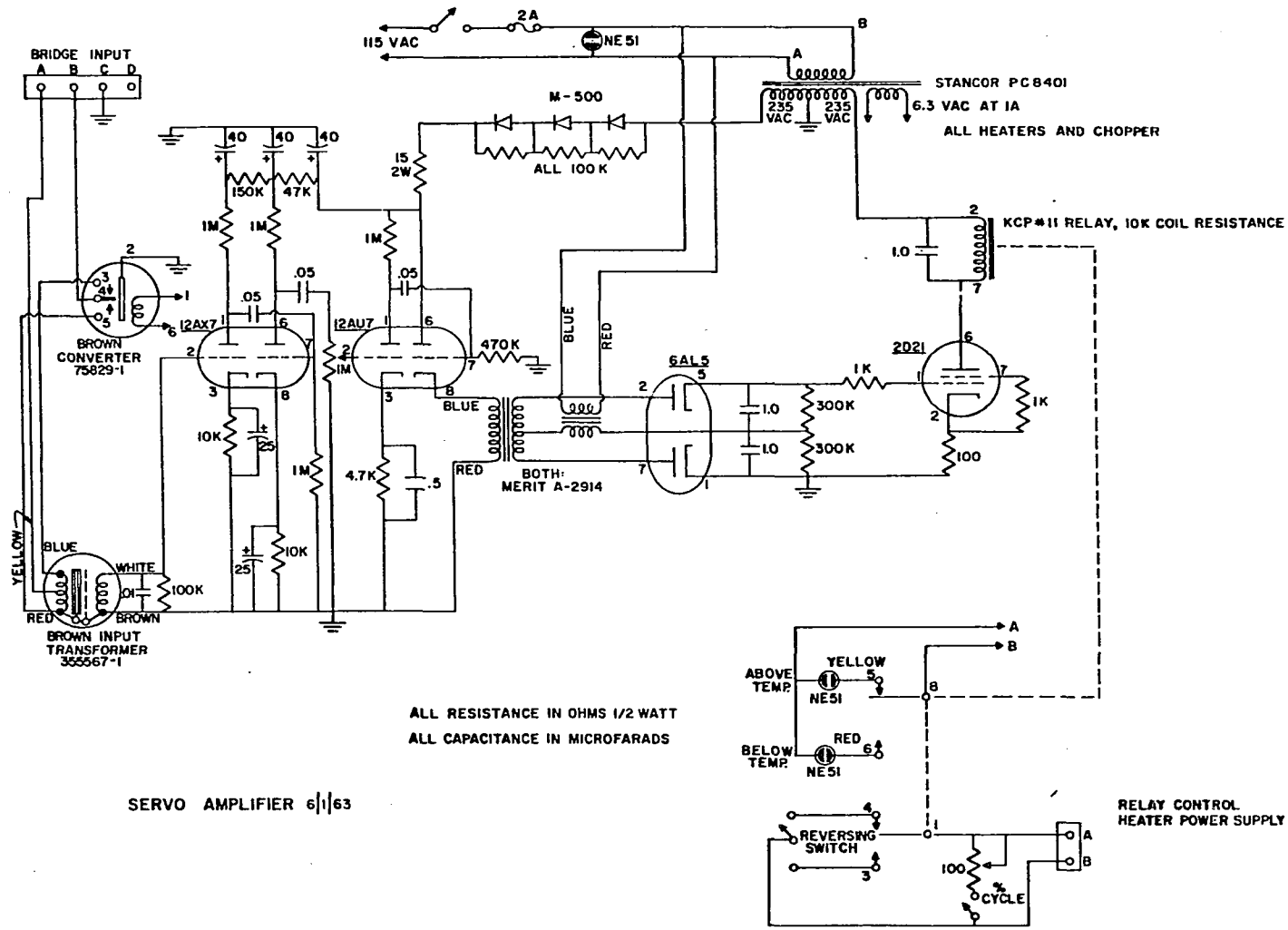

Figure 5. Diagram of temperature controller: Part I (servo amplifier)

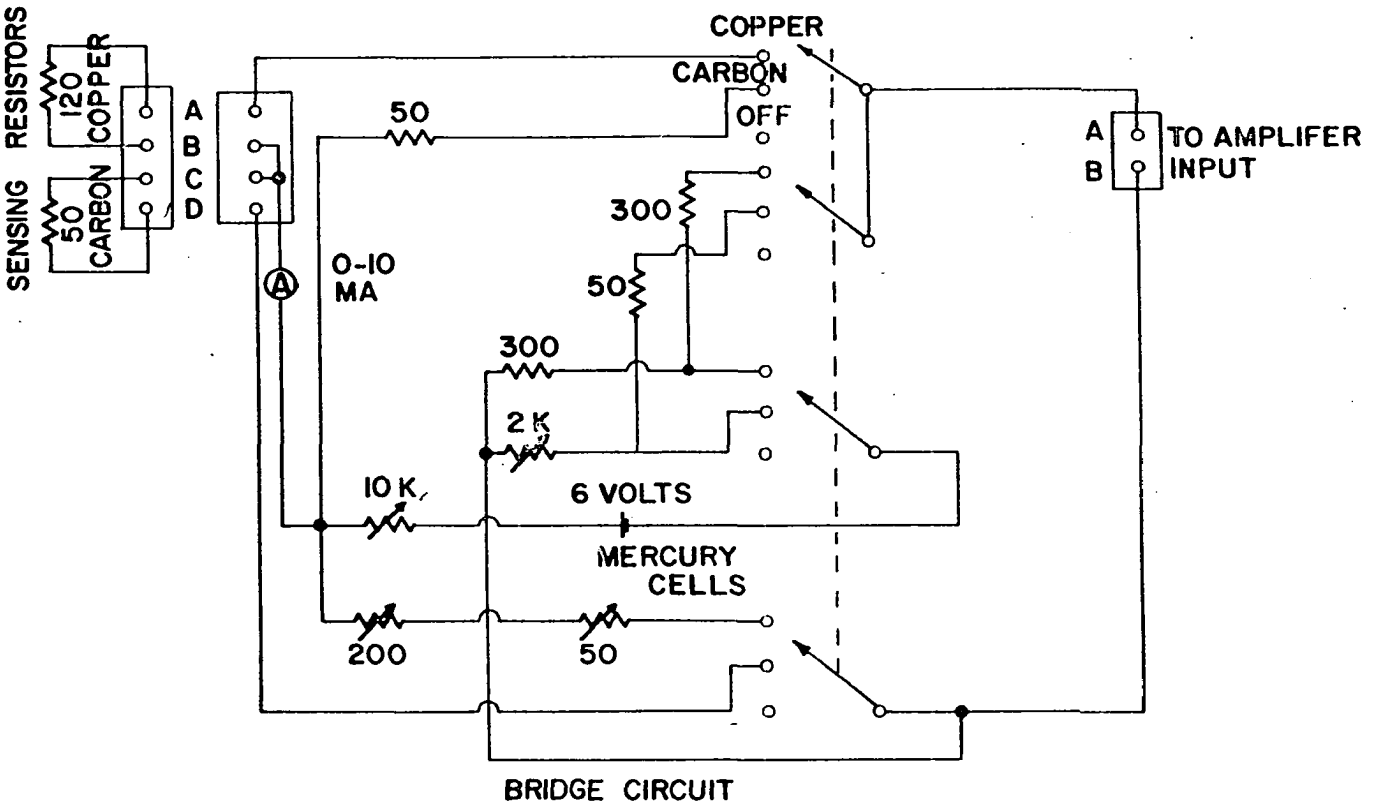

Figure 6. Diagram of temperature controller: Part II (bridge circuit)

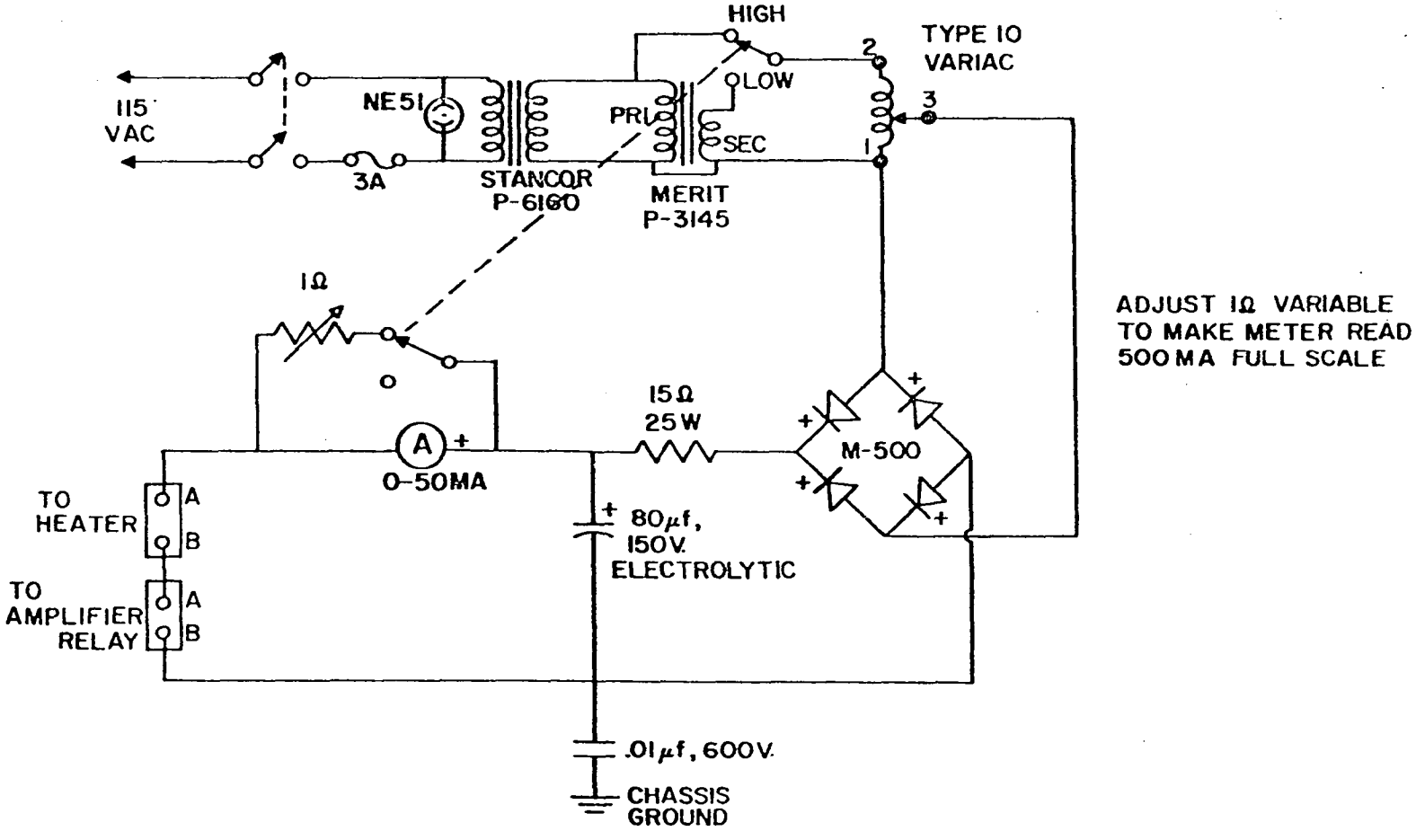

Figure 7. Diagram of temperature controller: Part III (heater power supply)

chamber. The off balance signal from the bridge was used to activate a relay which served as an on-off switch for the heater. Any desired temperature above bath could be achieved by an appropriate setting of the variable resistor in the Wheatstone bridge. In practice about 1 milliampere current was used in the bridge circuit.

Temperature measurements were made with gold + 0.03% iron vs. copper thermocouples from 4.2°K to 25°K. The sensitivity of these thermocouples is greater than 10 microvolts per degree in this region. The emf vs. T curve for these thermocouples was determined by Finnemore et al. (21) and was accurate to ± 0.1°K. The sensitivity was determined by fitting a third order polynomial to the emf vs. T curve and then differentiating directly.

Constantan vs. copper thermocouples were used in the temperature range 25°K to 450°K. The emf vs. T curve for these thermocouples was determined by calibration at the boiling points of helium, hydrogen, nitrogen, oxygen, and argon. The sensitivity of these thermocouples was determined in the same manner as for the gold + 0.03% iron vs. copper thermocouples and varied in magnitude from 7 microvolts per degree at 25°K to 40 microvolts per degree at 300°K. The technique used to determine the sensitivity of the thermo-

couples is similar to that given by Powell et al. (44).

The thermocouple voltages were measured with a Leeds and Northrup, type K-3 potentiometer with a Leeds and Northrup, type 9834, electronic galvanometer as the null detector. The emf could be read to ± 0.1 microvolt.

The thermocouples were soldered into small holes in the copper blocks at either end of the sample. These holes were placed about 0.5 mm from the ends of the sample. The potential leads were soldered between the ends of the sample and the copper block when the sample was initially mounted. Referring to Figure 3 we see that if there is a temperature difference, ΔT, between the ends of the sample we have

$$\Delta V_{AX} = S_{AX}\Delta T + e_1 \tag{35}$$

$$\Delta V_{AC} = S_{AC}\Delta T + e_2 \tag{36}$$

Where ΔV_{AX} is the voltage between the potential leads, ΔV_{AC} is the voltage difference between the upper and lower thermocouples, S_{AX} is the thermoelectric power of the sample relative to copper, S_{AC} is the sensitivity of the thermocouple at the average temperature of the sample, and e_1 and e_2 are extraneous voltages caused by thermals in the measuring circuit. By careful construction the extraneous voltages

were virtually eliminated. Thus from Equations 1 and 2 we obtain

$$S_{AX} = S_{AC} \Delta V_{AX}/\Delta V_{AC}. \quad (37)$$

Thus, since S_{AC} is known for the thermocouples used in this experiment, a measurement of ΔV_{AX} and ΔV_{AC} as a function of temperature gives S_{AX} as a function of temperature. To find the absolute thermoelectric power of a sample, the relative thermoelectric power between the copper wires in the apparatus and a sample of 99.999% pure lead, obtained from the American Smelting and Refining Corporation, was measured. Using the absolute thermoelectric power data of Christian et al. (15) for lead, the absolute thermoelectric power of the copper was then obtained.

By the definition $S_X = S_A - S_{AX}$, all the data needed to find S_X were then available.

The voltage ΔV_{AX} was measured with a Rubicon, model 2779, low microvolt potentiometer with a Sensitive Research, type 5214, photocell galvanometer amplifier and a secondary galvanometer, type SR21, as the null detector. This apparatus could measure changes of 0.01 microvolt from 0 to 200 microvolts.

Apparatus and Method for Electrical Resistivity Measurements

A standard four probe method was used to measure the electrical resistivities. The sample holder is shown in Figure 8. Razor blade edges, mounted in a section of red fibre board, were used as potential probes. The same heat leak chamber was used as for the thermoelectric power measurements. In this case a copper plate was soldered between the copper blocks. The sample was placed in good thermal contact with the copper plate but electrically insulated from it by a layer of etched printed circuit board. A phosphor bronze spring was used to hold the potential probes and sample in place.

The current leads were soldered to the sample at least a diameter of the sample from the potential probes. The measuring circuit is shown in Figure 8. The current was supplied by a lead-acid cell and was stable to 1 part in 10^4 over the time required for a measurement. The current was determined by measuring the emf across a 0.1 ohm standard resistor with a Leeds and Northrup, type K-3 potentiometer. In practice, currents of either 0.1000 ampere of 0.1500 ampere were used.

The voltage between the potential leads was measured

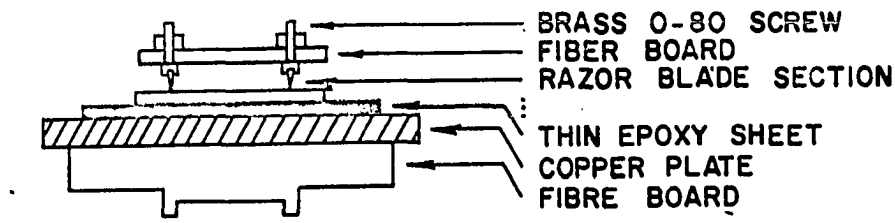

(a) SAMPLE HOLDER

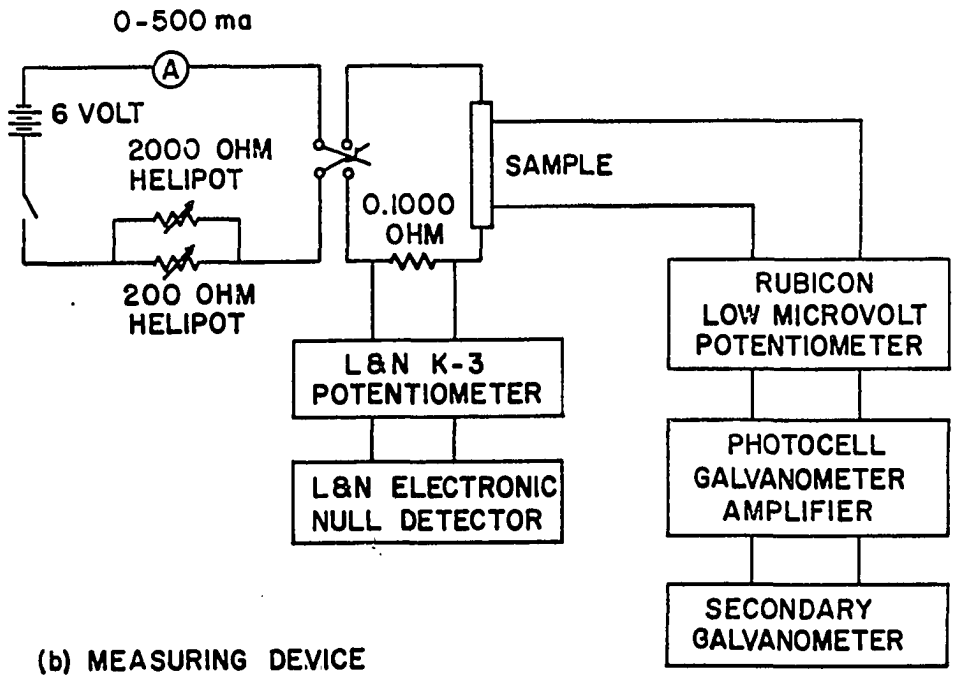

(b) MEASURING DEVICE

Figure 8. Sample holder and measuring circuit for electrical resistivity measurements

with the same rubicon low microvolt potentiometer and galvanometer amplifier which were used to measure the thermoelectric voltages.

Apparatus and Method for Field Cooling Measurements

Magnetic fields up to 28 kilogauss were produced by a Magnion, model UF-10-5, electromagnet and power supply. A conventional metal dewar was mounted between the poles of the electromagnet. The intensities of the magnetic fields were measured by a Rawson, Model 720, rotating coil gaussmeter. For the high field measurements a Magnion, model CF50-100-500, superconducting solenoid with a Magnion, model CFC-5, power supply was used. The solenoid was capable of producing a maximum field of 55 kilogauss and was operated in the persistent mode. The intensities of the magnetic fields were determined by measuring the voltage drop across a 0.1 ohm standard resistor in series with the solenoid. The coil constant was supplied by the manufacturer. The one-inch bore solenoid was placed in a metal dewar which had a capacity of about 5 liters of liquid helium.

The sample holder used for this work is shown in Figure 9. A standard four probe method was used to measure the electrical resistance as a function of temperature and

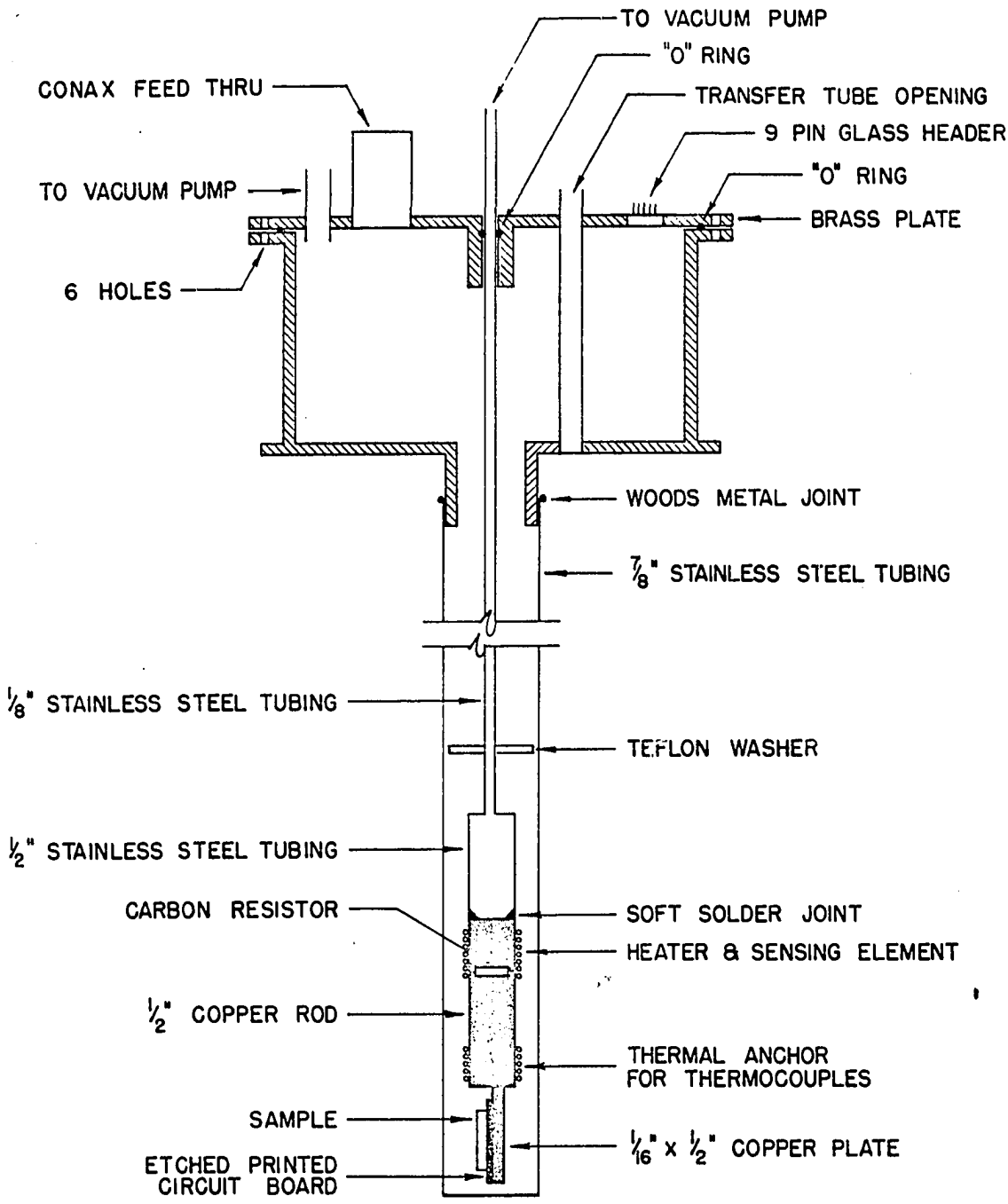

Figure 9. Sample holder for field cooling measurements

magnetic field. AWG #38, copper potential leads were soldered to the sample. The thermocouples, heaters, and sensing elements were the same in this sample holder as those used in the thermoelectric power sample holder. The outer shell of the sample holder was a 7/8 inch, non-magnetic stainless steel tube. For the low field measurements, a liquid nitrogen bath was used and the sample holder was evacuated to a pressure of 10^{-3} torr. For the high field measurements a problem was encountered. Because of space limitations the sample holder had to be immersed directly in the liquid helium bath in the bore of the solenoid. However, the experimental procedure required that the sample be cooled from 325°K in a magnetic field. This was accomplished by using Teflon spacers and evacuating the sample chamber to 10^{-5} torr before inserting it into the liquid helium bath. Thus, heat input into the cryostat was reduced to a level which allowed a reasonable amount of time to take measurements and also prevented the solenoid from heating above its quenching temperature. The procedure was to heat the sample to 325°K, energize the solenoid, and then allow the sample to cool at about 2°K per minute to 273°K. Data was then taken while increasing temperature.

The potentiometers, temperature control system, and current supply were the same as those used for the electrical resistivity measurements.

Errors in Transport Property Measurements

The electrical resistivity is computed from the equation

$$\rho = V/I \; A/L. \tag{38}$$

Thus, the fractional error is

$$\delta\rho/\rho = [(\delta V/V)^2 + (\delta I/I)^2 + (\delta A/A)^2 + (\delta L/L)^2]^{1/2}. \tag{39}$$

The relative error is determined by the first two terms. The emf was measured to within 0.02% and thermal emfs were eliminated by reversing the current. The current was stable to within 0.04% over the period of one measurement and was adjusted before each measurement. Thus, the relative error is approximately 0.05%. Other factors contributing to the relative error are the lack of steady state conditions and errors in temperature measurement. The lack of steady state conditions would lead to random errors which are small, as evidenced by the lack of scatter in the data. The temperature control equipment, however, was capable of reducing the

drift to less than $0.01^{o}K$ over the time required to make the measurement. The absolute value of the temperatures were accurate to $\pm$ $0.1^{o}K$ from $4.2^{o}K$ to $30^{o}K$ and to $\pm$ $0.5^{o}K$ above $30^{o}K$. The thermocouples were quite reproducible and the relative error in temperature measurement is estimated to be $\pm$ $0.1^{o}K$. The absolute error is determined by the last two terms in Equation 39. The length is estimated to be accurate to 1% while the measurement of the cross sectional area can be in error by as much as 5%. The absolute error is therefore about 6%.

The relative thermoelectric power is determined from the equation

$$S_{AX} = S_{AC}\, \Delta V_{AX}/\Delta V_{AC}. \tag{40}$$

The fractional error is then

$$\delta S_{AX}/S_{AX} = [(\delta S_{AC}/S_{AC})^2 + (\delta(\Delta V_{AX})/\Delta V_{AX})^2 + (\delta(\Delta V_{AC})/\Delta V_{AC})^2]^{1/2}. \tag{41}$$

As mentioned in the section on experimental methods, S_{AC} was determined by differentiating the curve of emf versus T. There can be two sources of error for S_{AC}. The first error

comes from the initial computation of S_{AC}. This is estimated to be 1% at 30°K and decreasing to about 0.02% at room temperature. The second error arises due to the uncertainty in the absolute temperature which then leads to an error in determining S_{AC} from the curve of S_{AC} versus T. The second error is largest at 30°K and is about 1% at that temperature.

Errors in ΔV_{AX} can occur because of inaccuracy of measuring instruments, because of extraneous emfs in the circuit, and because of temperature gradients which might exist between the potential leads and the ends of the sample. The accuracy of the potentiometer was certified by the manufacturer as 0.02% and the null detector was sufficiently sensitive to achieve this accuracy. The extraneous thermal emfs were kept to a minimum by careful construction. With no temperature gradient across the sample at 4.2°K, ΔV_{XC} was found to be 0.30 ± 0.1 μV. This zero point reading was taken before beginning each run and was found to be almost constant. At liquid nitrogen temperatures the extraneous thermal emf was found to be 0.15 ± 0.05 μV. Because these thermal emfs remained fairly constant, they cancel out of the absolute thermoelectric power to a large degree since the same thermal emf was present in the calibration of the potential leads with the lead sample. The temperature

gradients between the potential leads and the ends of the sample were eliminated partially by thermally anchoring the potential leads and partially by soldering the potential leads to the ends of the sample.

The largest source of error in S_{AX} is in the determination of the quantity ΔV_{AC}. This can occur because of mismatch of thermocouples or because the thermocouples are not measuring the correct temperature. The error due to this mismatch can easily be determined and was found to be 5% below 30°K, 1% below 77°K and gradually becoming negligible at about 200°K. In order to ensure that the thermocouples were sensing the correct temperature they were (a) thermally anchored at the sample temperature (b) soldered to the ends of the sample and (c) all measurements were made in a vacuum of about 10^{-5} torr. The error in the actual measurement of ΔV_{AC} was less than 1%. The errors in the temperature measurements are the same as given for the electrical resistivity. The errors, of course, were also present in the calibration run so there is an additional uncertainty in the absolute thermoelectric power.

In summary, the absolute error is estimated to be about 5% below 30°K gradually decreasing to about 1% at about 77°K

and remaining constant above this temperature with the condition that the absolute error is probably never smaller than $\pm$ 0.1 μV.

As evidenced by the lack of scatter in the data, the relative error is small and is estimated to be $\pm$ 0.05 μV.

EXPERIMENTAL RESULTS

Electrical Resistivities of Dilute Chromium Alloys

The electrical resistivities of Cr - 0.10%V, Cr - 0.50%V, and Cr - 1.00%V single crystals as a function of temperature from 4.2°K to 320°K are shown in Figure 10. The resistivities of Cr - 1.50%V, Cr - 2.00%V, and Cr - 3.00%V single crystals as a function of temperature from 4.2°K to 300°K are shown in Figure 11. The humps which occur in the curves are interpreted as arising from the onset of antiferromagnetism.

For all of the above samples the magnetic ordering occurred in the region where the resistivity would normally be expected to vary linearly with temperature. About 5 or 10 degrees above the Néel temperature the resistivity does indeed become linear with temperature. Therefore, a straight line which has been fitted to the data above T_N can be extrapolated below the Néel temperature and should be a fairly reasonable estimate of the contribution of the phonon scattering to the resistivity. The difference between the actual resistivity and the straight line should then represent $\rho-\rho_{ph}$. This procedure was carried out by using a least

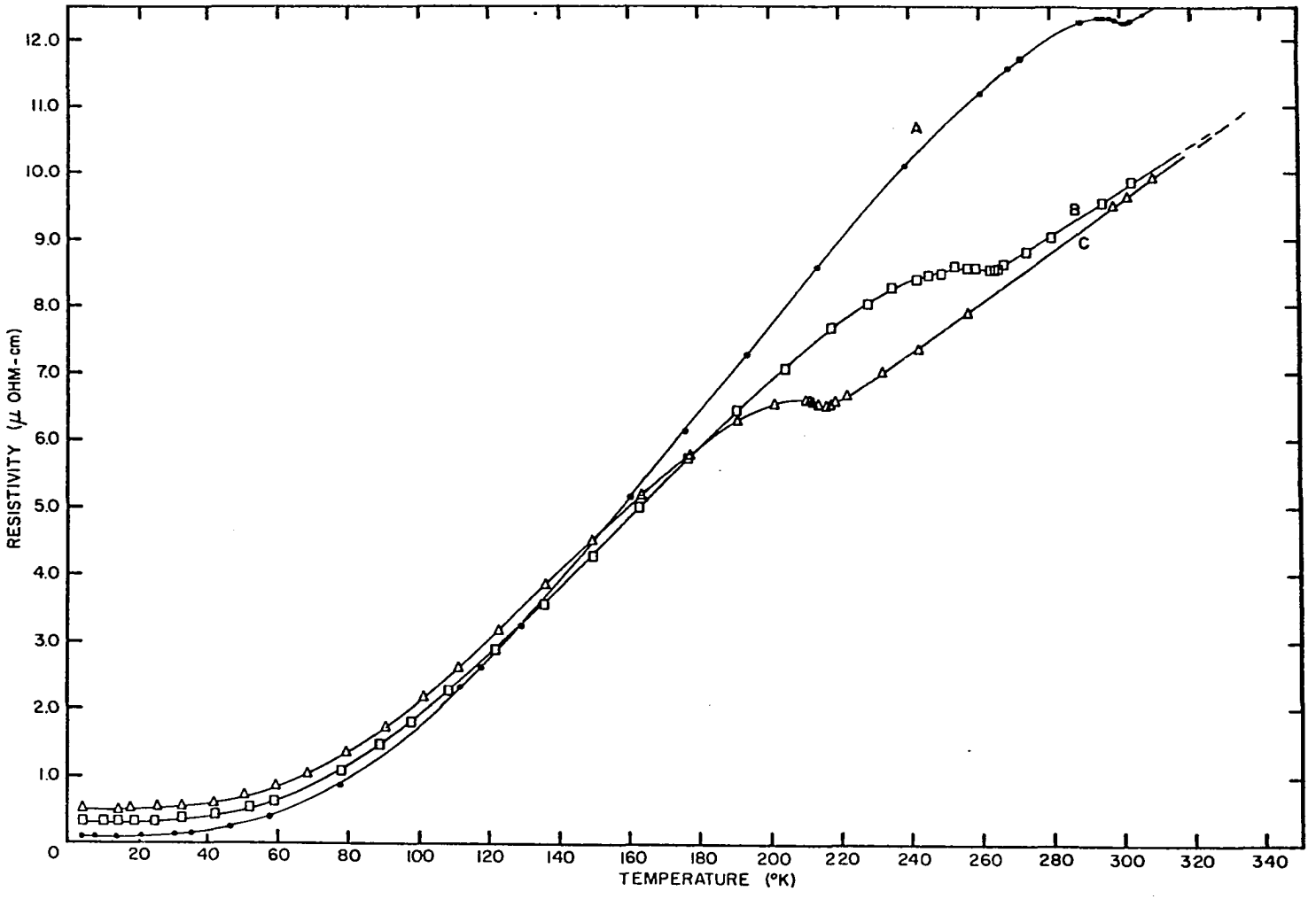

Figure 10. Electrical resistivity versus temperature for Cr - V alloys: Part I (A. Cr - 0.10%V; B. Cr - 0.50%V; C. Cr - 1.00% V)

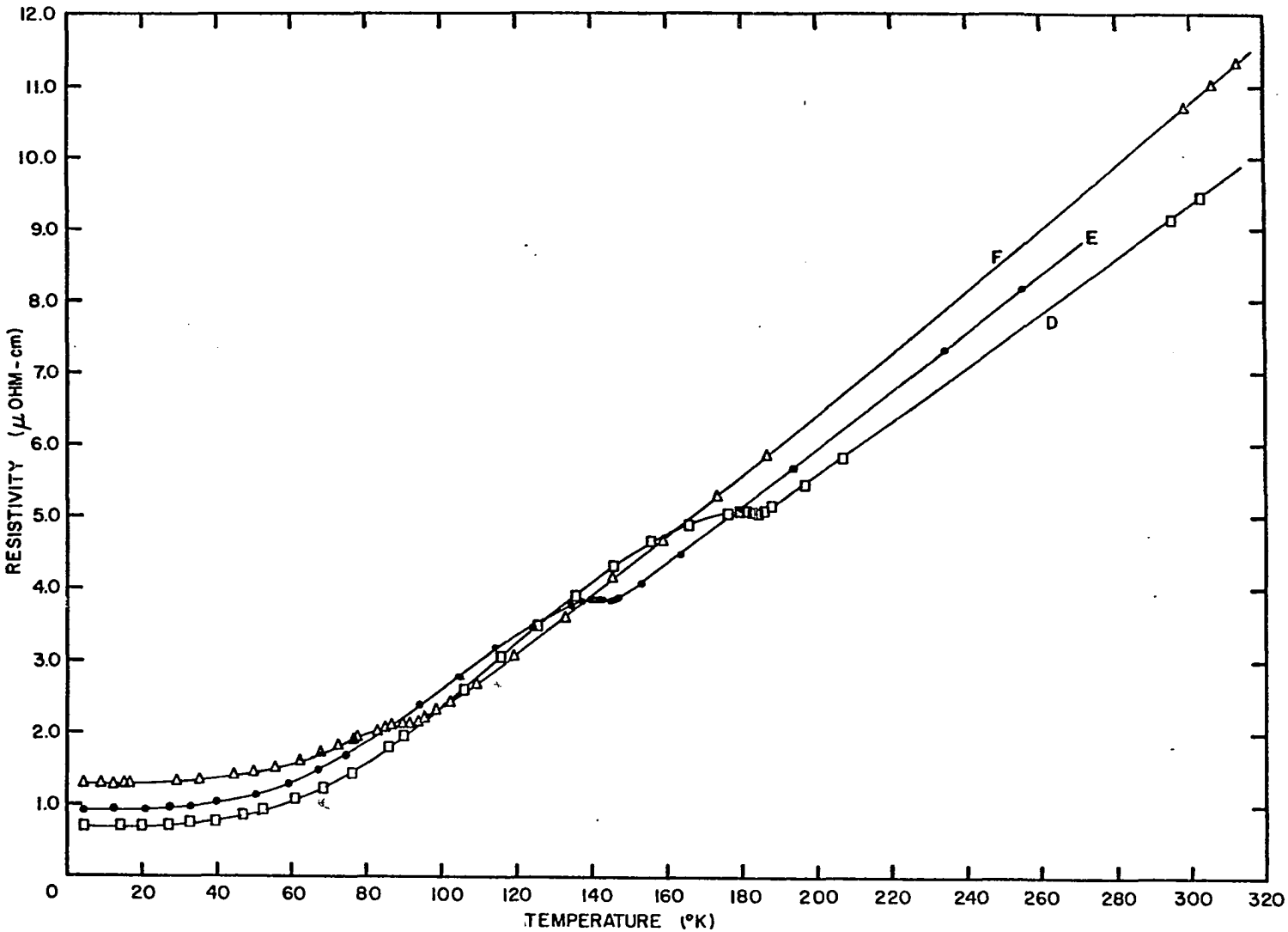

Figure 11. Electrical resistivity versus temperature for Cr - V alloys: Part II (D. Cr - 1.50%V; E. Cr - 2.00%V; F. Cr - 2.80% V)

squares fit to the data above T_N to determine the analytical equation of the straight line. The difference between the actual curve and this straight line was then determined for each data point by actual computation. The entire procedure was carried out on an IBM 7074 Computer. The magnetic contributions to the resistivities of these alloys are shown in Figure 13. The parameter $\alpha = (\rho - \rho_{ph})/\rho_{ph}$ was also determined as a part of the same program and is shown for each of the alloys in Figure 14.

The electrical resistivities of Cr - 3.00%V, Cr - 3.15%V and Cr - 4.65%V single crystals as functions of temperature are shown in Figure 12. The Cr - 4.65%V crystal does not show any evidence of magnetic ordering. The minima in the curves for Cr - 3.15%V and Cr - 3.00%V are interpreted as being due to magnetic ordering. For these two samples the ordering takes place in the residual resistance region and the contribution of the magnetic ordering to the electrical resistivity is readily apparent.

It should be noted that the relative error is very much smaller than the absolute error due mainly to difficulties in measuring the cross sectional areas of the samples.

The resistivities of Cr - 0.35%Mn, Cr - 0.09%Re and

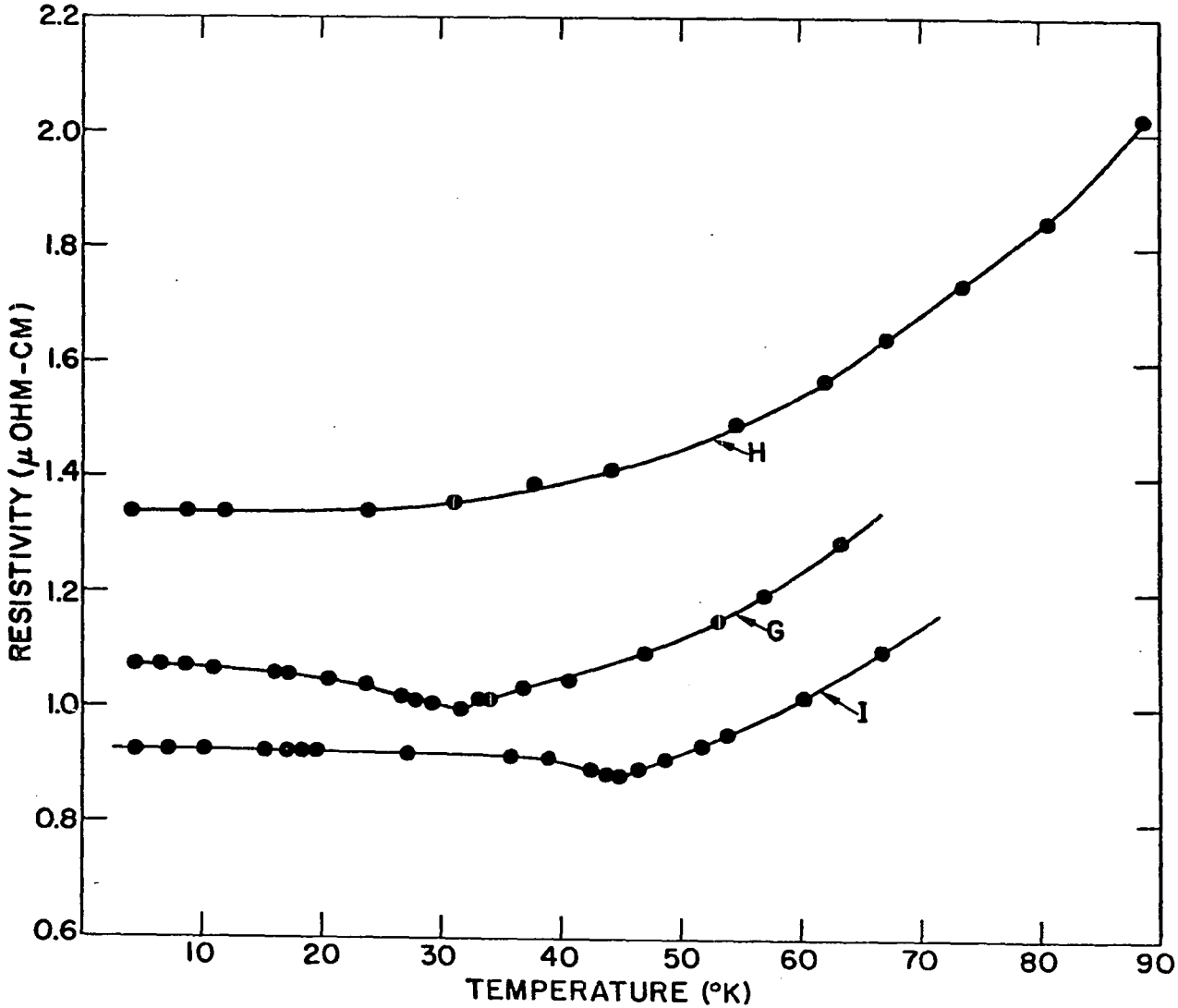

Figure 12. Electrical resistivity versus temperature for Cr - V alloys: Part III (H. Cr - 4.65%V; G. Cr - 3.15%V; I. Cr - 3.00% V)

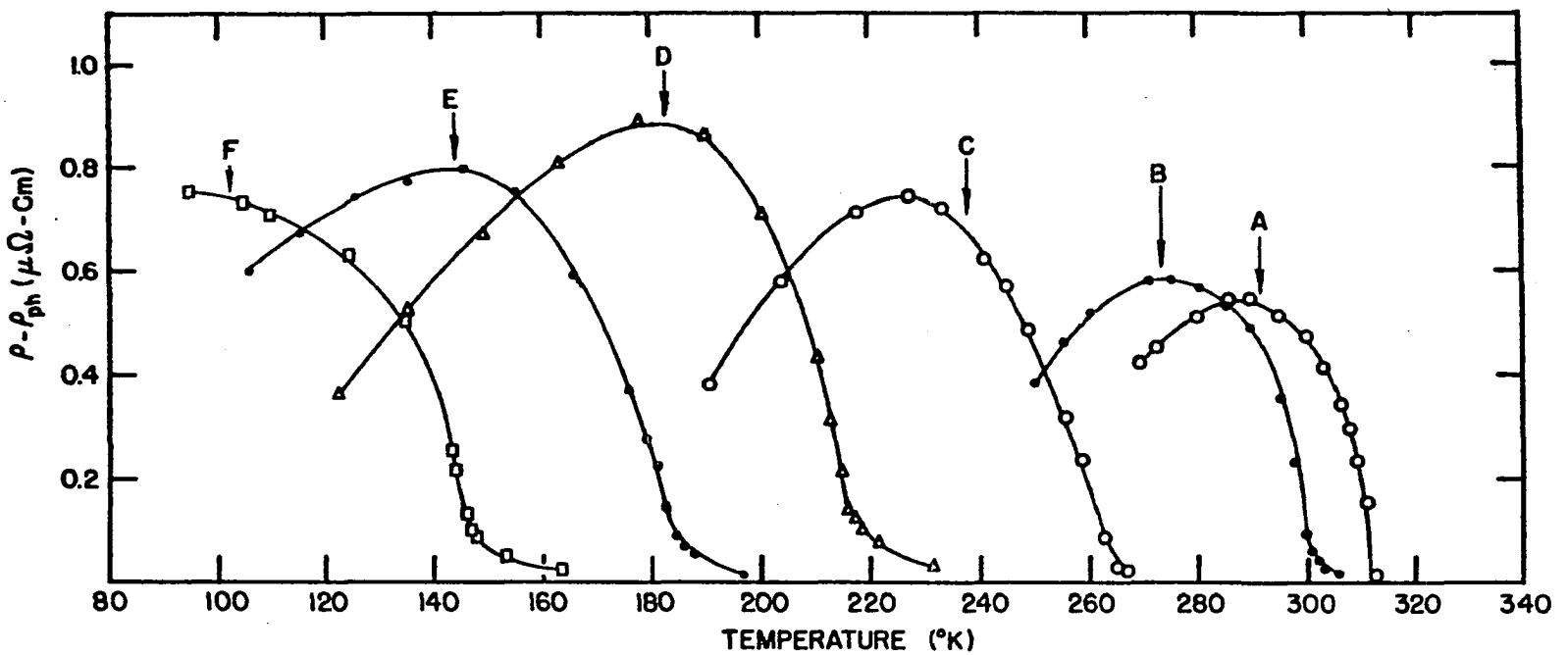

Figure 13. Curves of ($\rho - \rho_{ph}$) versus temperature (A. pure Cr; B. Cr - 0.10%V; C. Cr - 0.50%V; D. Cr - 1.00%V; E. Cr - 1.50% V; F. Cr - 2.00%V)

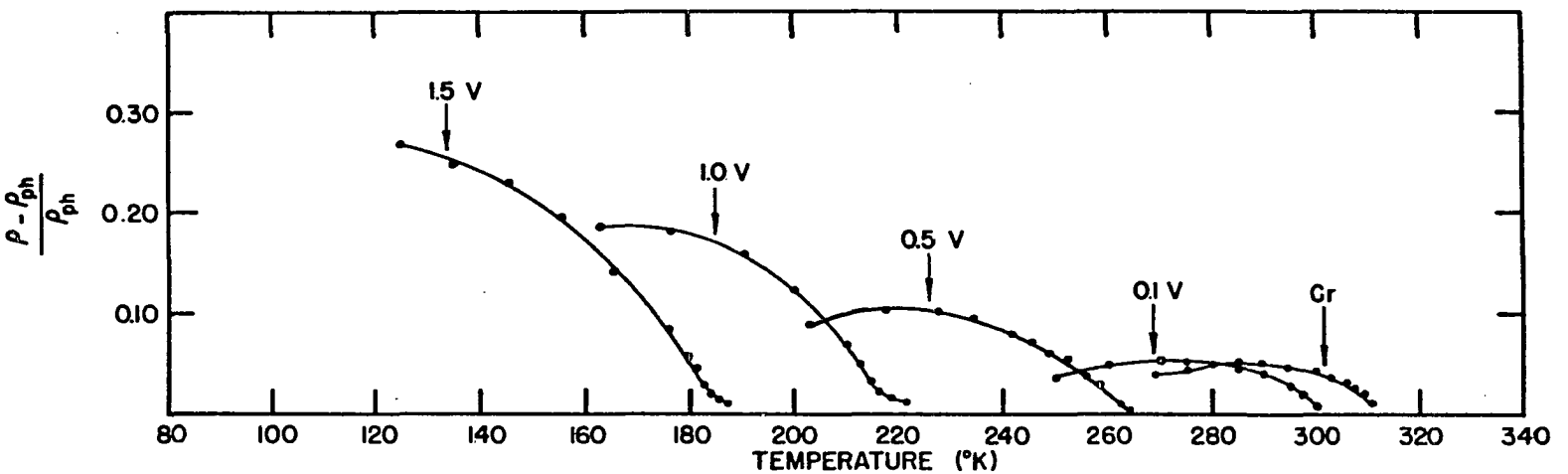

Figure 14. Curves of $(\rho - \rho_{ph})/\rho_{ph}$ versus temperature

Cr - 0.19%Re are shown as a function of temperature in Figure 15. The humps in the curves are again interpreted as arising from magnetic ordering.

Thermoelectric Powers of Dilute Chromium Alloys

The thermoelectric powers of Cr - 0.10%V, Cr - 0.50%V and Cr - 1.00%V as functions of temperature from 10°K to 320°K are shown in Figure 16. The curves of thermoelectric power versus temperature all have a maximum similar to that found for pure chromium (36). The change of slope about 30°K above the maximum is interpreted as occurring at the Néel temperature. The thermoelectric powers of two samples of Cr - 0.10%V were measured and the resulting curves were identical within the experimental error. The thermoelectric powers of two different samples of Cr - 1.00%V were also measured. The results were identical within the experimental error below 160°K and differed by about 8% above this temperature. The magnitude of the anomaly was the same for the two curves, however, and the Néel temperatures were the same so only one curve is plotted. The thermoelectric powers of Cr - 1.50%V, Cr - 2.00%V, Cr - 2.50%V and Cr - 4.65%V as functions of temperature from 10°K to 300°K are shown in Figure 17. The curves for the Cr - 1.50%V, Cr - 2.00%V, and

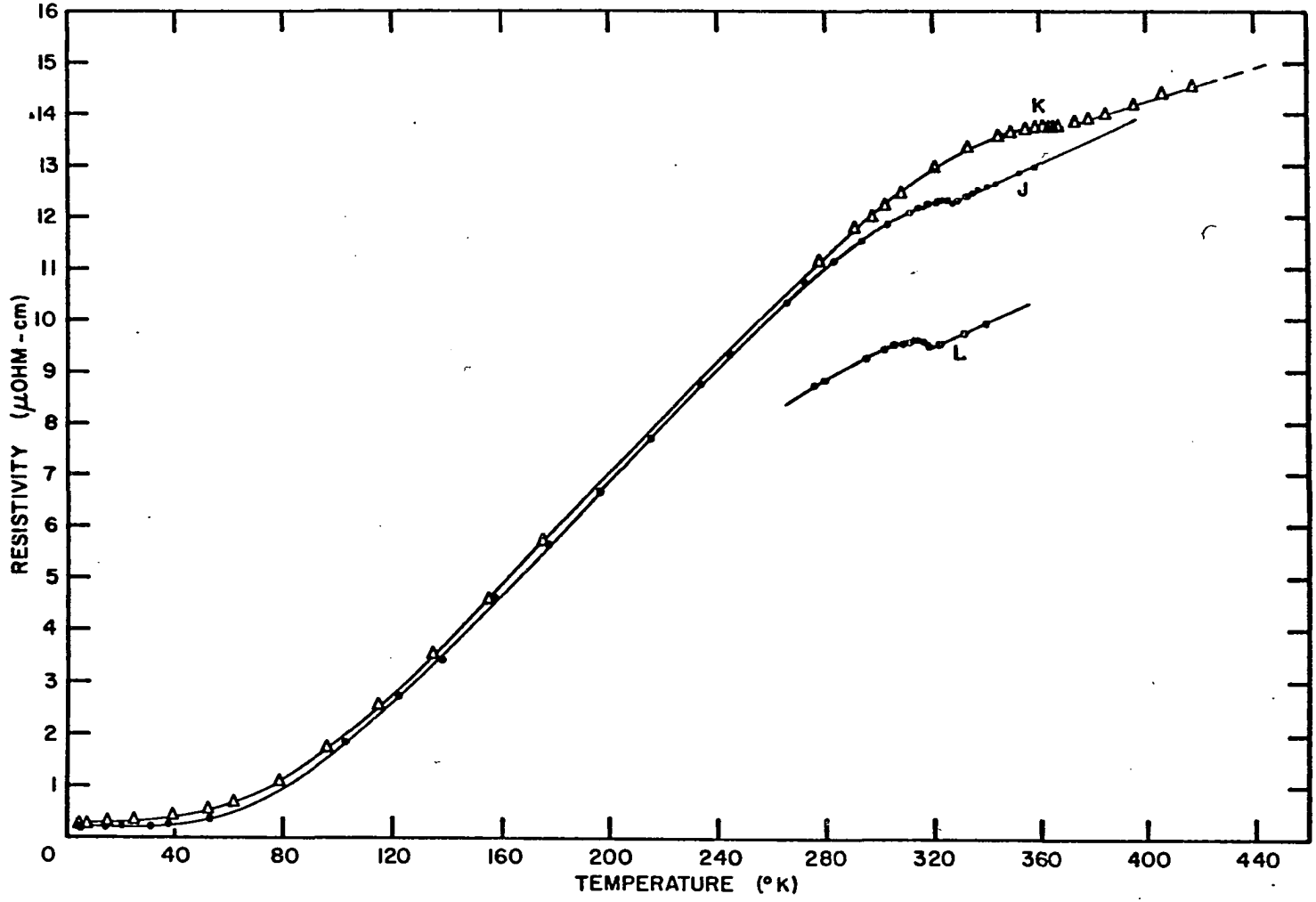

Figure 15. Electrical resistivity versus temperature for Cr - Re and Cr - Mn alloys (K. Cr - 0.35 At.%Mn; J. Cr - 0.19 At.%Re; L. Cr - 0.09 At.%Re)

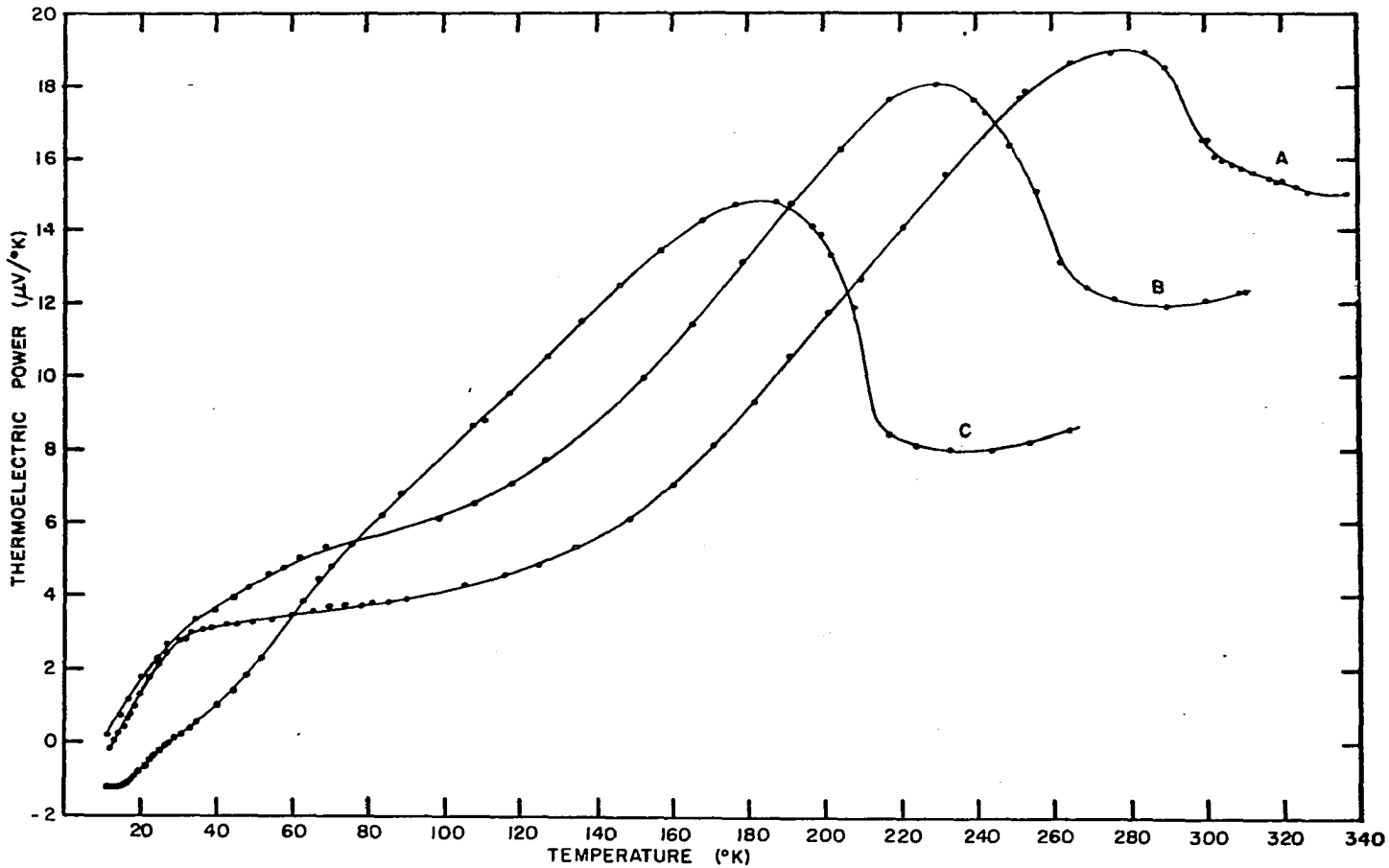

Figure 16. Absolute thermoelectric power versus temperature for Cr - V alloys: Part I (A. Cr - 0.10%V; B. Cr - 0.50%V; C. Cr - 1.00%V)

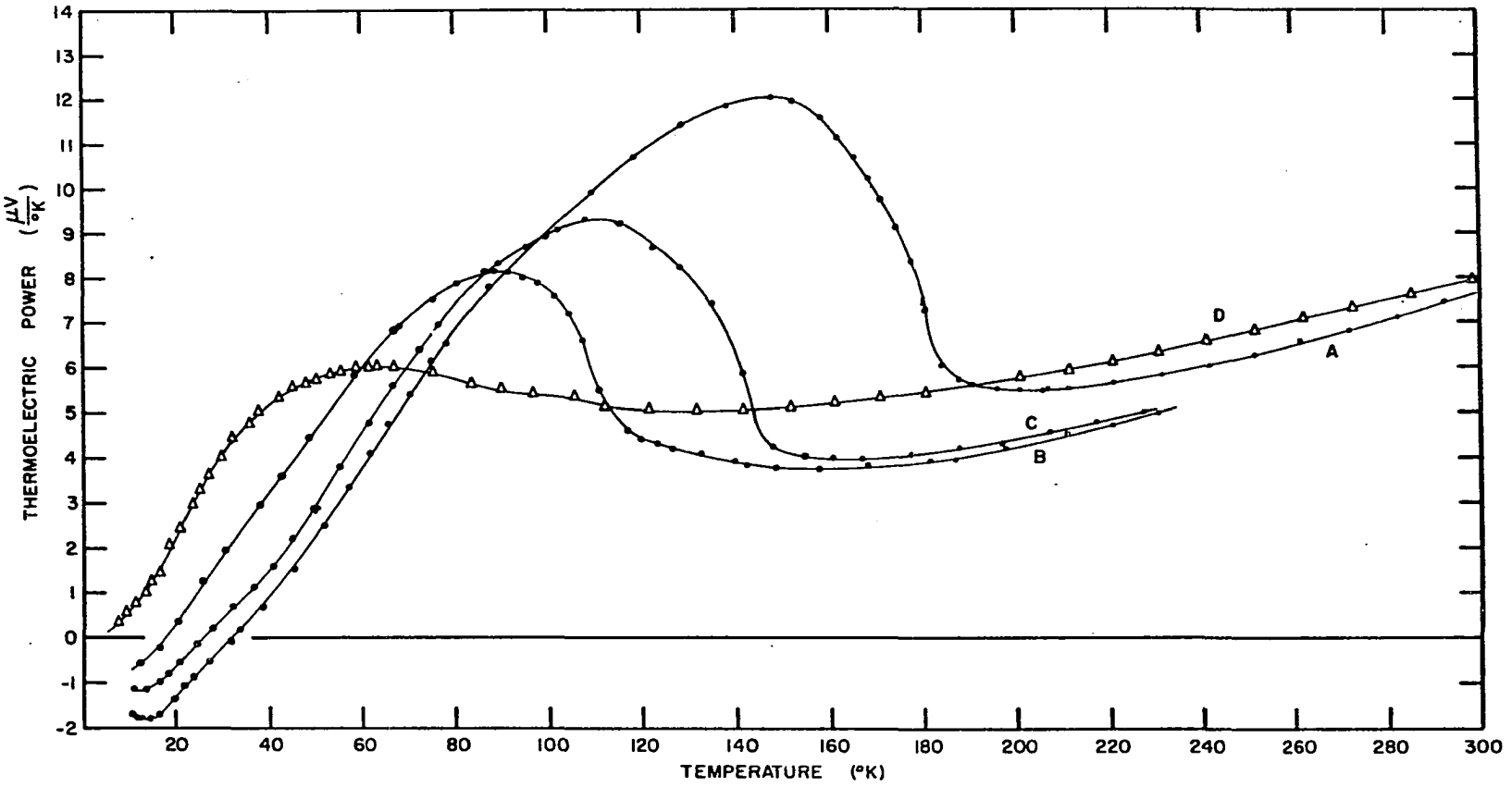

Figure 17. Absolute thermoelectric power versus temperature for Cr - V alloys: Part II (A. Cr - 1.50%V; B. Cr - 2.50%V; C. Cr - 2.00%V; D. Cr - 4.65%V)

Cr - 2.50%V samples show the characteristic hump due to the onset of antiferromagnetism while the maximum in the curve for the Cr - 4.65%V sample is interpreted as arising from phonon drag.

The thermoelectric powers of Cr - 3.15%V and Cr - 2.80%V single crystals as functions of temperature are shown in Figure 18. No evidence of magnetic ordering is seen in the curve for Cr - 3.15%V although the curve of electrical resistivity versus temperature clearly showed an anomaly at about 28°K. The maximum in the Cr - 2.80%V sample occurs at a temperature where the maximum of the phonon drag component occurred in non-ordered samples. However, part of the contribution to the hump arises from magnetic ordering, as evidenced by the sharp decrease and change of slope which would not occur if phonon drag were the only mechanism. Evidence of magnetic ordering for this sample was also seen in the curve of electrical resistivity versus temperature.

The thermoelectric power of a Cr - 3.00%V single crystal as a function of temperature is shown in Figure 19. The maximum due to magnetic ordering and the maximum due to phonon drag have separated with a small minima in between. In this case it is extremely difficult to determine the Néel tempera-

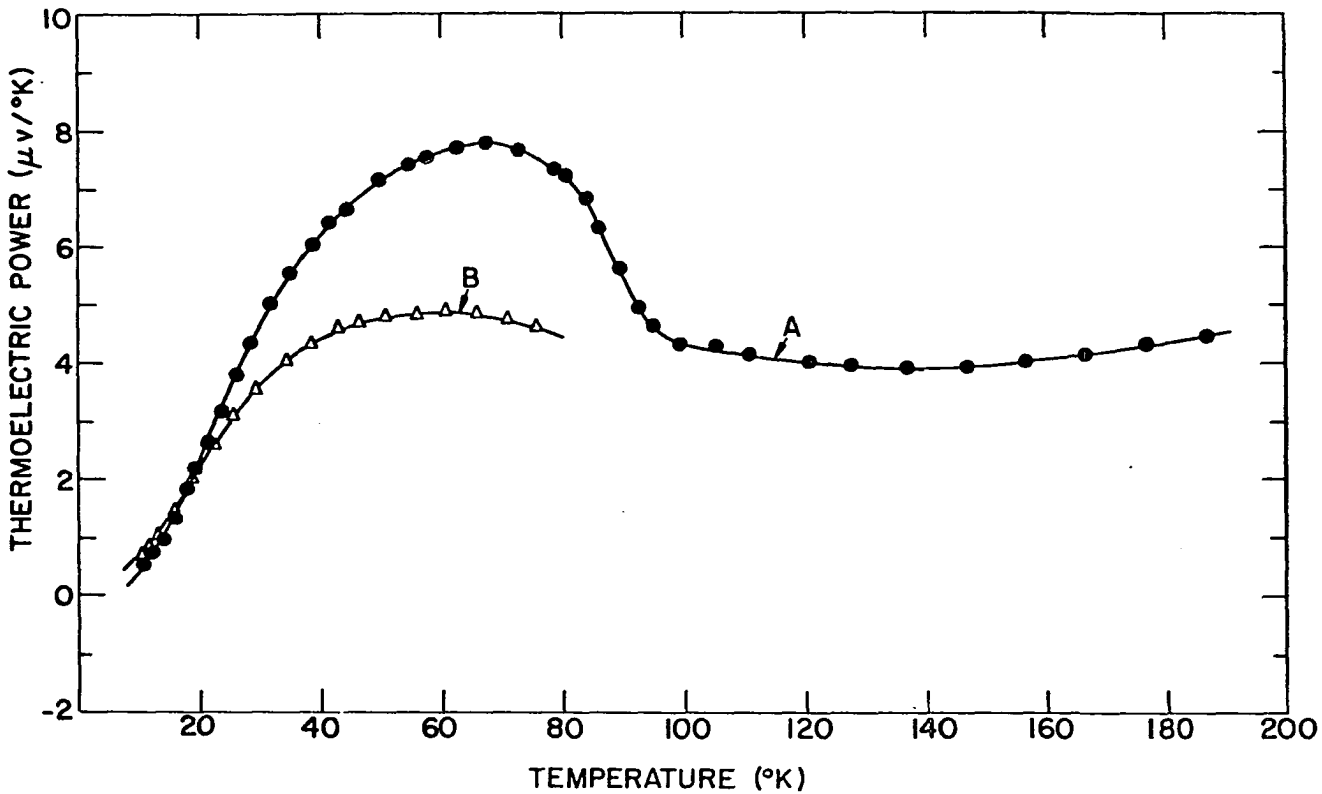

Figure 18. Absolute thermoelectric power versus temperature for Cr - V alloys: Part III (A. Cr - 2.80%V; B. Cr - 3.15%V)

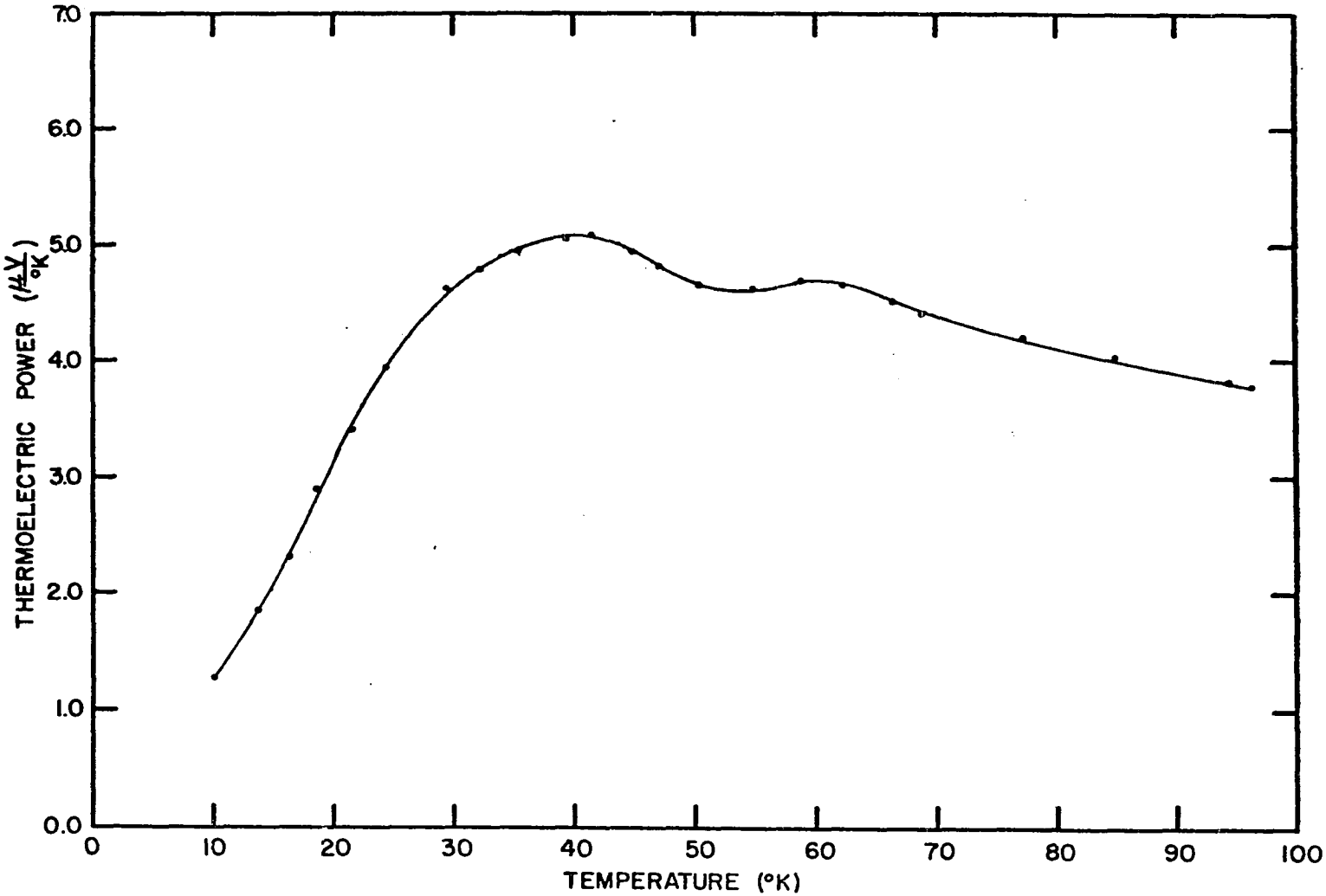

Figure 19. Absolute thermoelectric power versus temperature for Cr - 3.00%V

ture of the sample from the curves.

For the crystals from 0.50%V to 2.80%V it is seen that above the Néel temperature the thermoelectric power rapidly becomes linear. In fact, it was found that above the Néel temperature the thermoelectric power could be fitted by a straight line which passed through the origin. The linear fit was made by using a least squares analysis and the analytical form of the straight line determined. The magnetic contribution was then computed for each data point by subtracting the actual value of S from the computed value of S_{diff} at that temperature. The quantity $(S - S_{diff})/S_{diff}$ was also determined. The entire process was carried out on an IBM 7074 Computer. The results of these calculations are shown in Figures 20 and 21.

The thermoelectric powers of Cr - 0.08%Mn, Cr - 0.35%Mn, Cr - 0.96%Mn, Cr - 1.76%Mn, and Cr - 2.16%Mn, single crystals are shown as functions of temperature in Figure 22. Only the Cr - 0.08%Mn and Cr - 0.35%Mn samples show evidence of magnetic ordering. For all curves a maximum occurs at about $60^{o}K$ which is probably due to phonon drag or magnon drag contributions.

The thermoelectric powers of Cr - 0.07%Re and Cr -

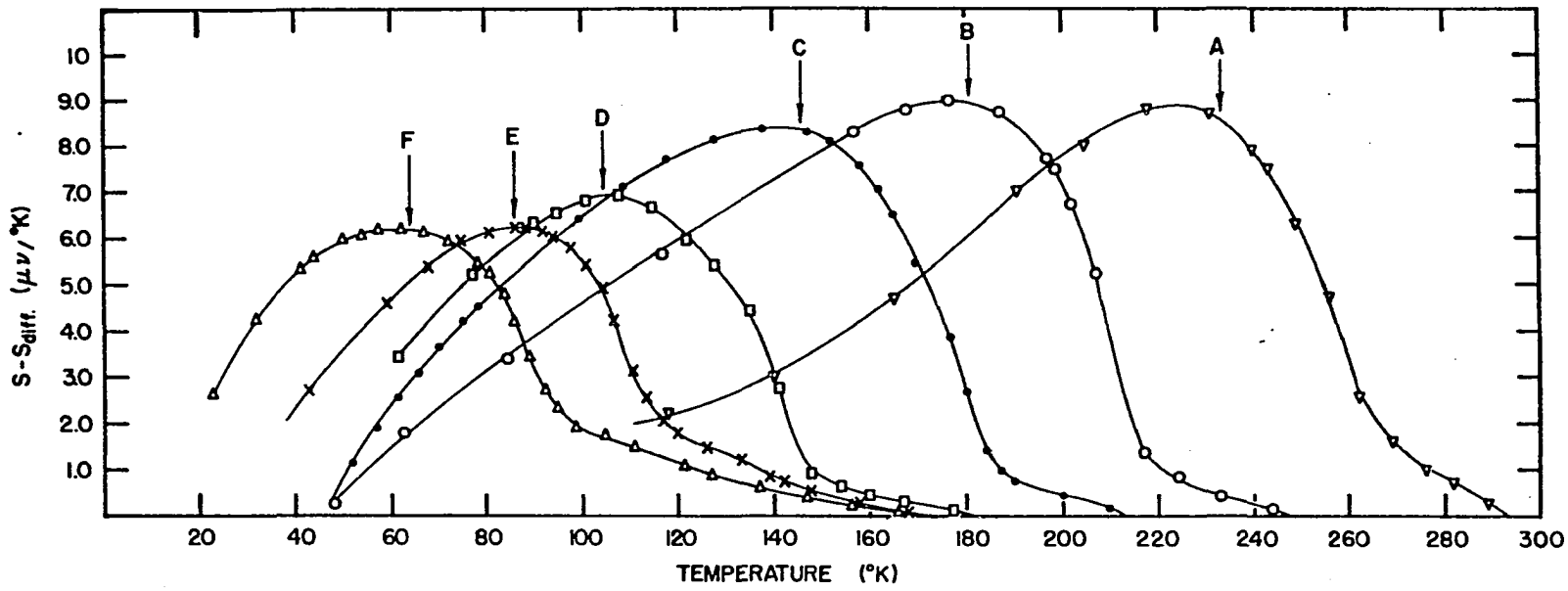

Figure 20. Curves of S - S_{diff} versus temperature for Cr - V alloys (A. Cr - 0.50%V; B. Cr - 1.00%V; C. Cr - 1.50%V; D. Cr - 2.00%V; E. Cr - 2.50%V; F. Cr - 2.80%V)

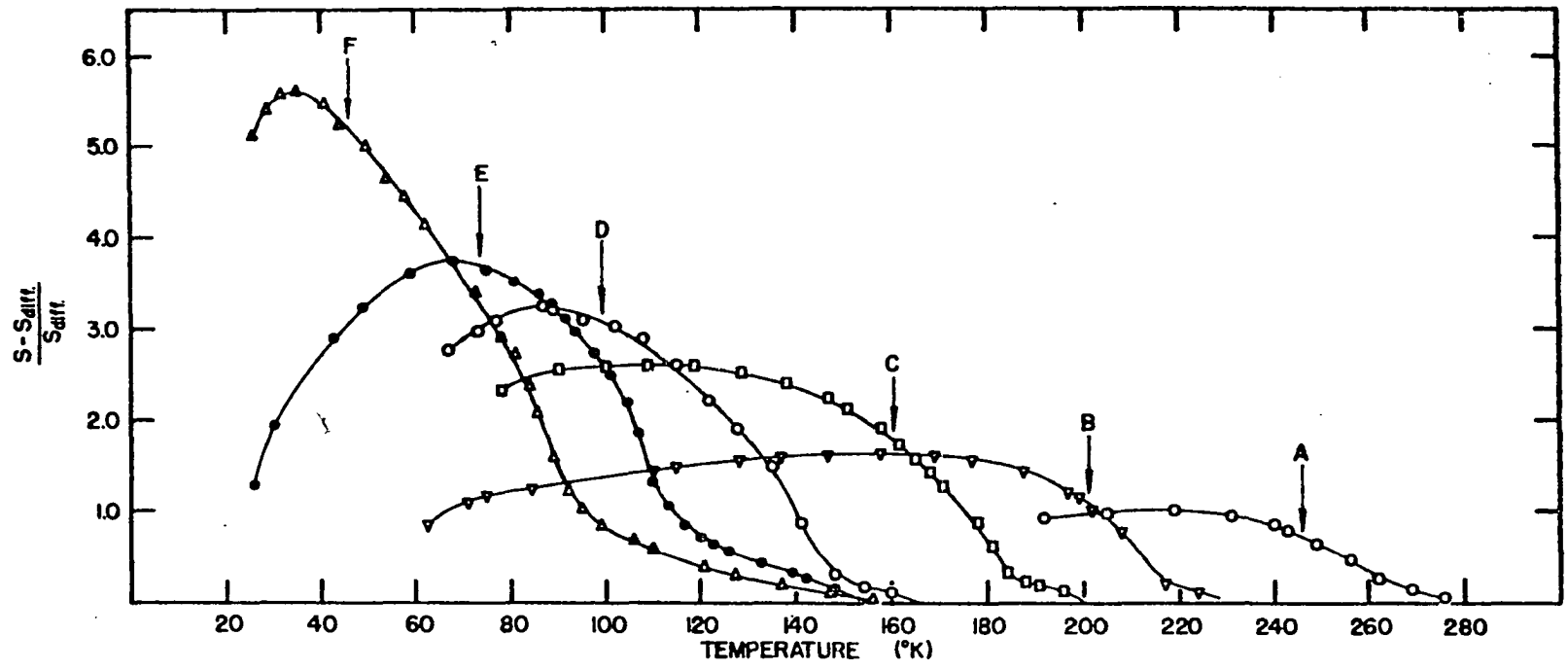

Figure 21. Curves of $(S - S_{diff})/S_{diff}$ versus temperature for Cr - V alloys (A. Cr - 0.50%V; B. Cr - 1.00%V; C. Cr - 1.50%V; D. Cr - 2.00%V; E. Cr - 2.50%V; F. Cr - 2.80%V)

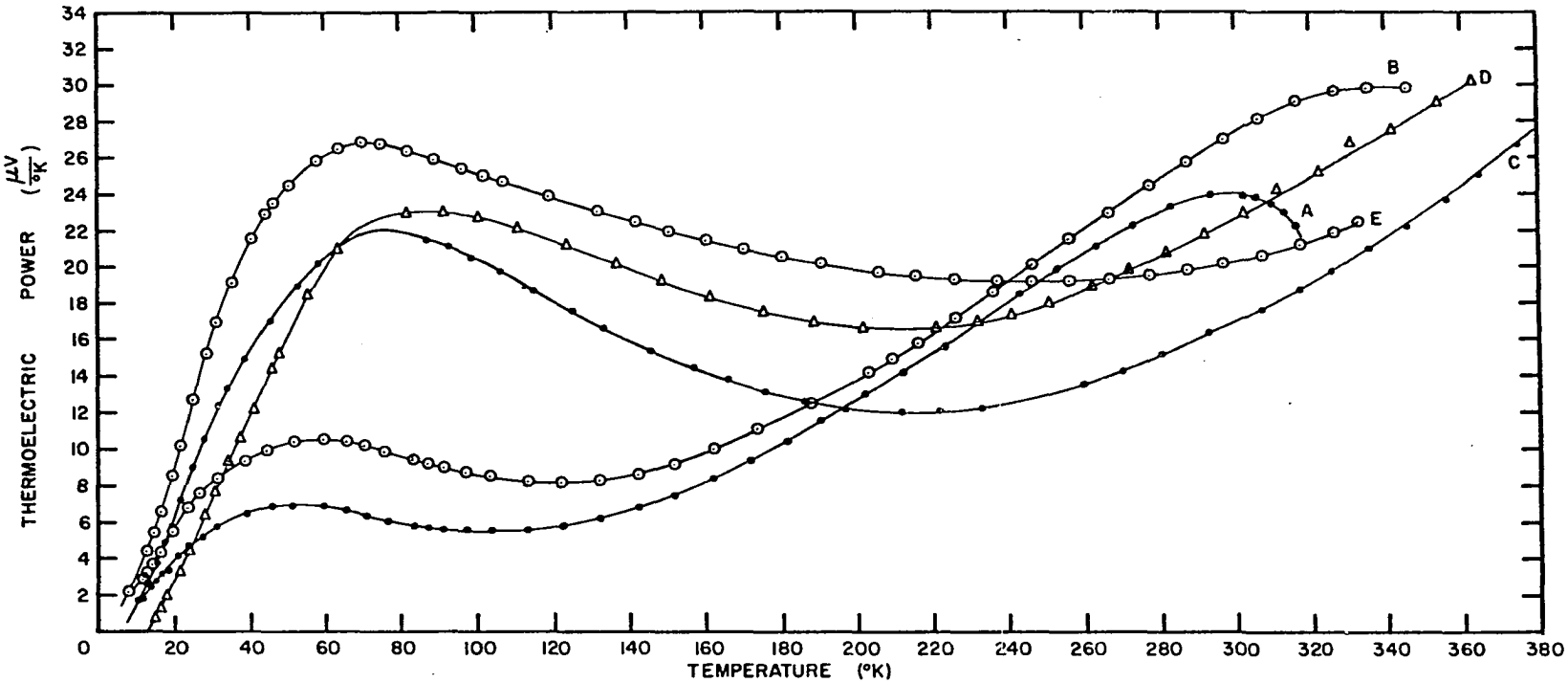

Figure 22. Absolute thermoelectric power of Cr - Mn alloys as a function of temperature (A. Cr - 0.08%Mn; B. Cr - 0.35%Mn; C. Cr - 1.76%Mn; D. Cr - 0.96%Mn; E. Cr - 2.16%Mn)

0.09%Re single crystals are shown in Figure 23. The Néel temperatures are taken to be at 316°K and 320°K respectively. The shape of these curves is very similar to the curve for pure Cr which is also plotted in this figure. The small secondary humps just above T_N are probably due to inhomogeneities in these crystals. Single crystals of Cr-Re alloys are extremely difficult to grow because of the large difference in melting point between rhenium and chromium. The higher melting point of the alloys increases the difficulty of removing the strains from the sample without the vaporization and hence loss of chromium. The Néel temperatures for all alloys studied are shown in Figure 24.

Effects of Field Cooling in Pure Chromium

The electrical resistivity as a function of temperature for a single crystal of pure Cr cooled through its Néel temperature in a magnetic field, H_c, of 28 kilogauss is shown in Figure 25. The long axis of the sample, which was in the form of a rectangular parallepiped, was parallel to [001].

The current direction was always parallel to the long axis with the cooling fields being applied either parallel to the long axis (longitudinal case) or at right angles to

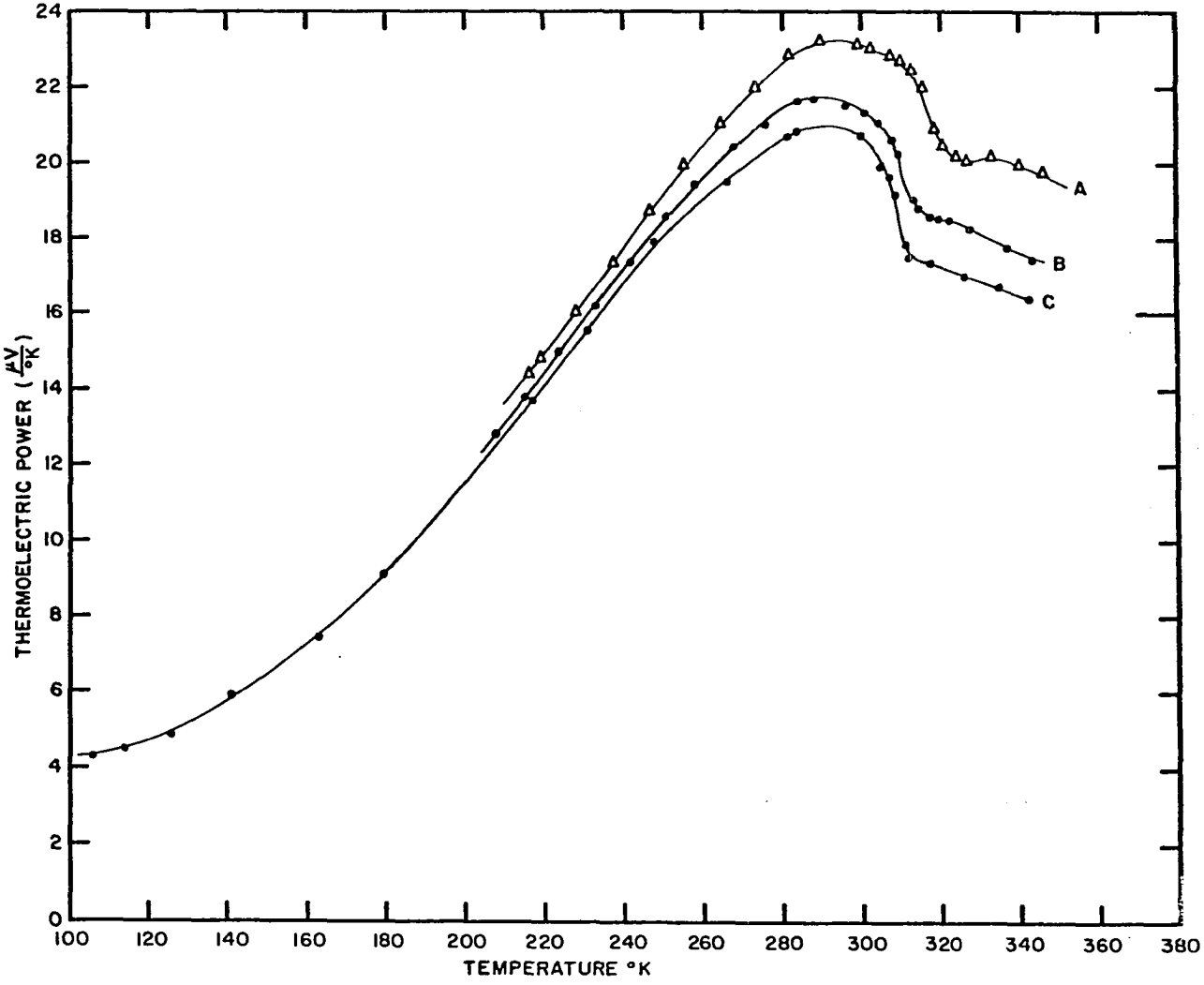

Figure 23. Absolute thermoelectric power of Cr - Re alloys as a function of temperature (A. Cr - 0.07 At.%Re; B. Cr - 0.09 At.%Re; C. pure Cr)

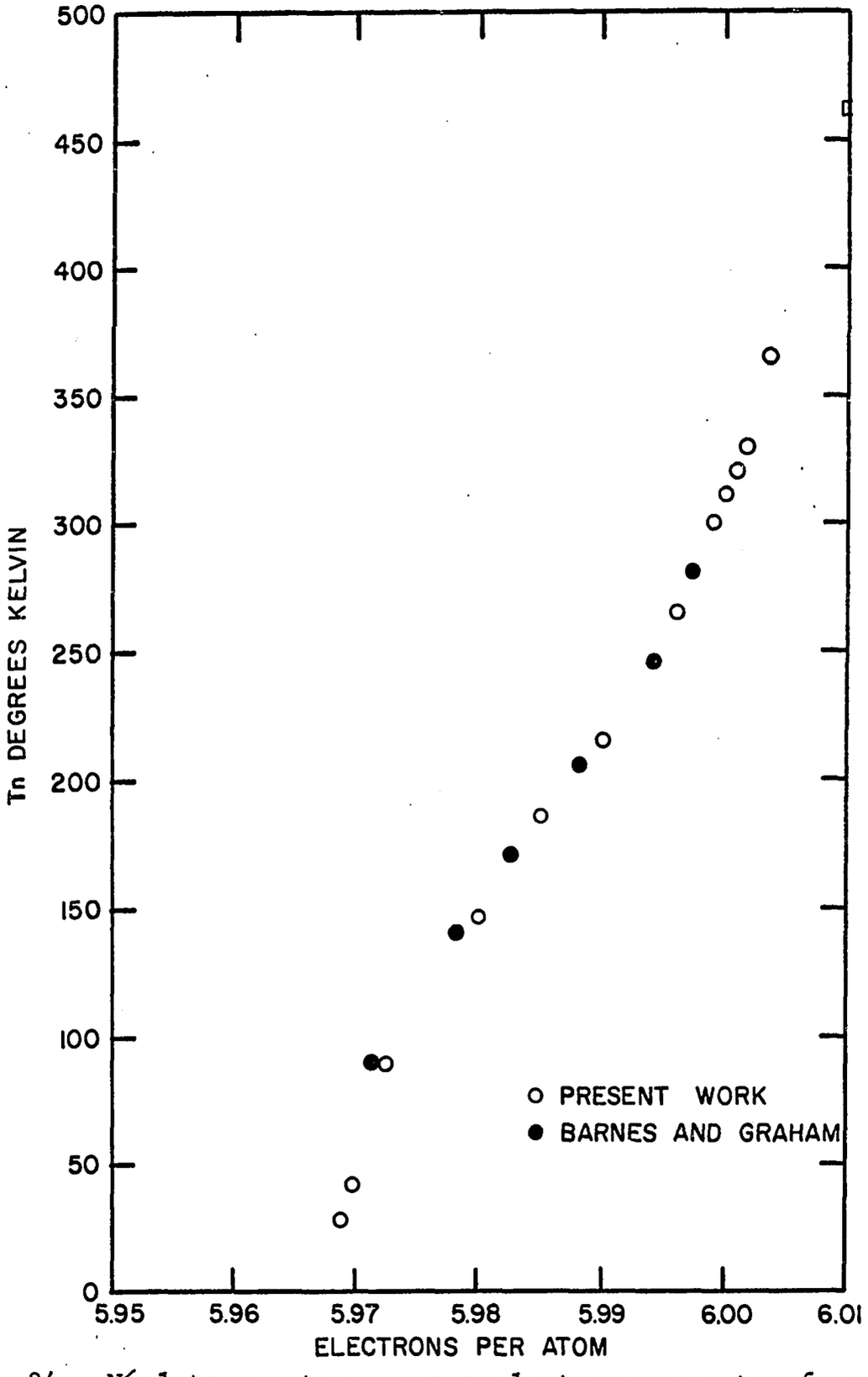

Figure 24. Néel temperature versus electrons per atom for dilute chromium alloys

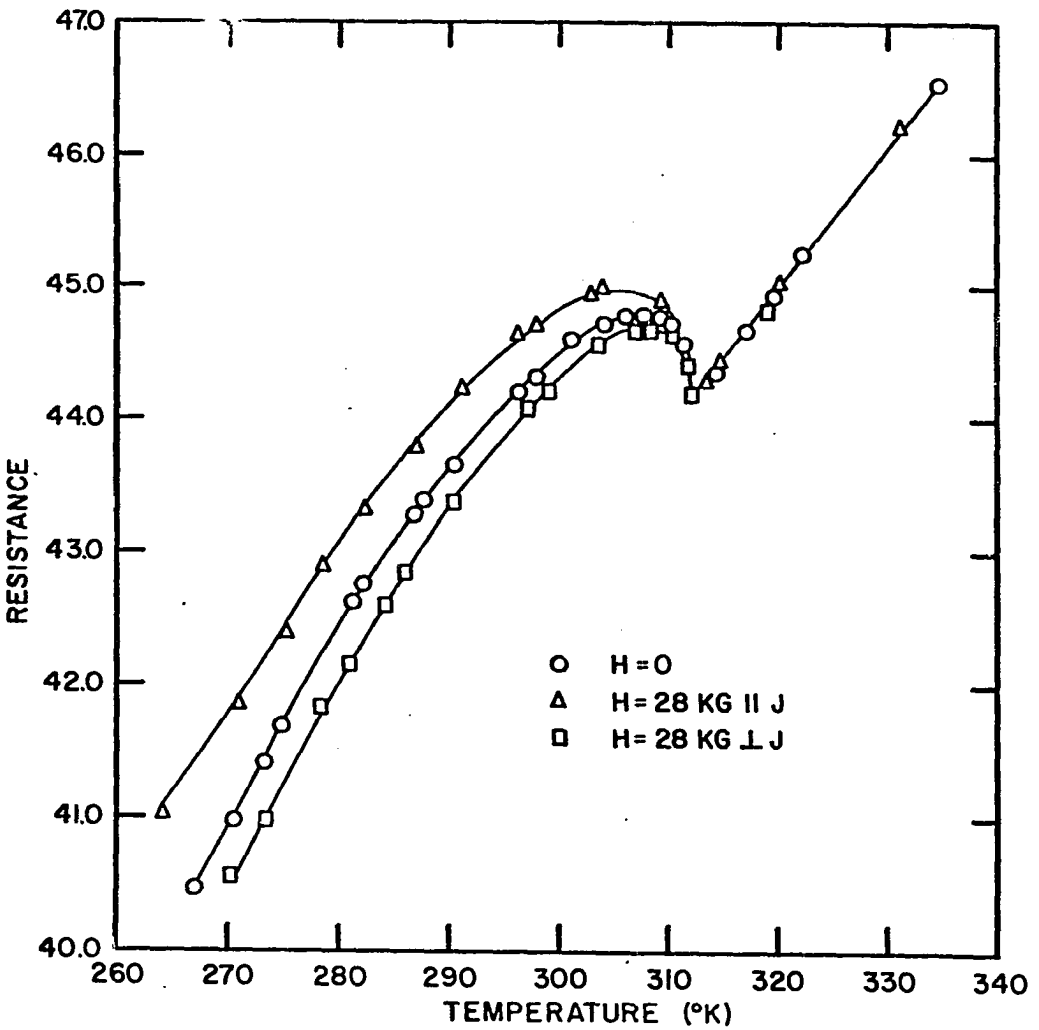

Figure 25. Electrical resistance versus temperature for field cooled specimens of pure Cr

the long axis but still parallel to a [100] or [010] axis (transverse case). The curves of electrical resistivity versus temperature are seen to lie above or below the zero cooling field curve depending upon field direction when the temperature is less than 312°K. Above 312°K the points all lie on one curve. In order to get reproducible results it was necessary to start each run at about 325°K. A curve for $H_c = 0$ was taken before and after the run for which $H_c \neq 0$. For all results shown the curves for $H_c = 0$ were reproducible. The initial measurements shown in Figure 25 were repeated in order to be sure that the effect was really due to the magnetic field and was not simply a result of thermal hysteresis. The data points above 312°K are important because without these one cannot be sure that a simple displacement of the curves has not occurred.

The same direction of the crystal was used for all longitudinal cooling fields while two different directions were used for transverse cooling fields.

The field cooling magnetoresistance curves are shown in Figure 26 for magnetic fields up to 55 kilogauss. Longitudinal cooling fields give a positive effect while transverse cooling fields give a negative effect.

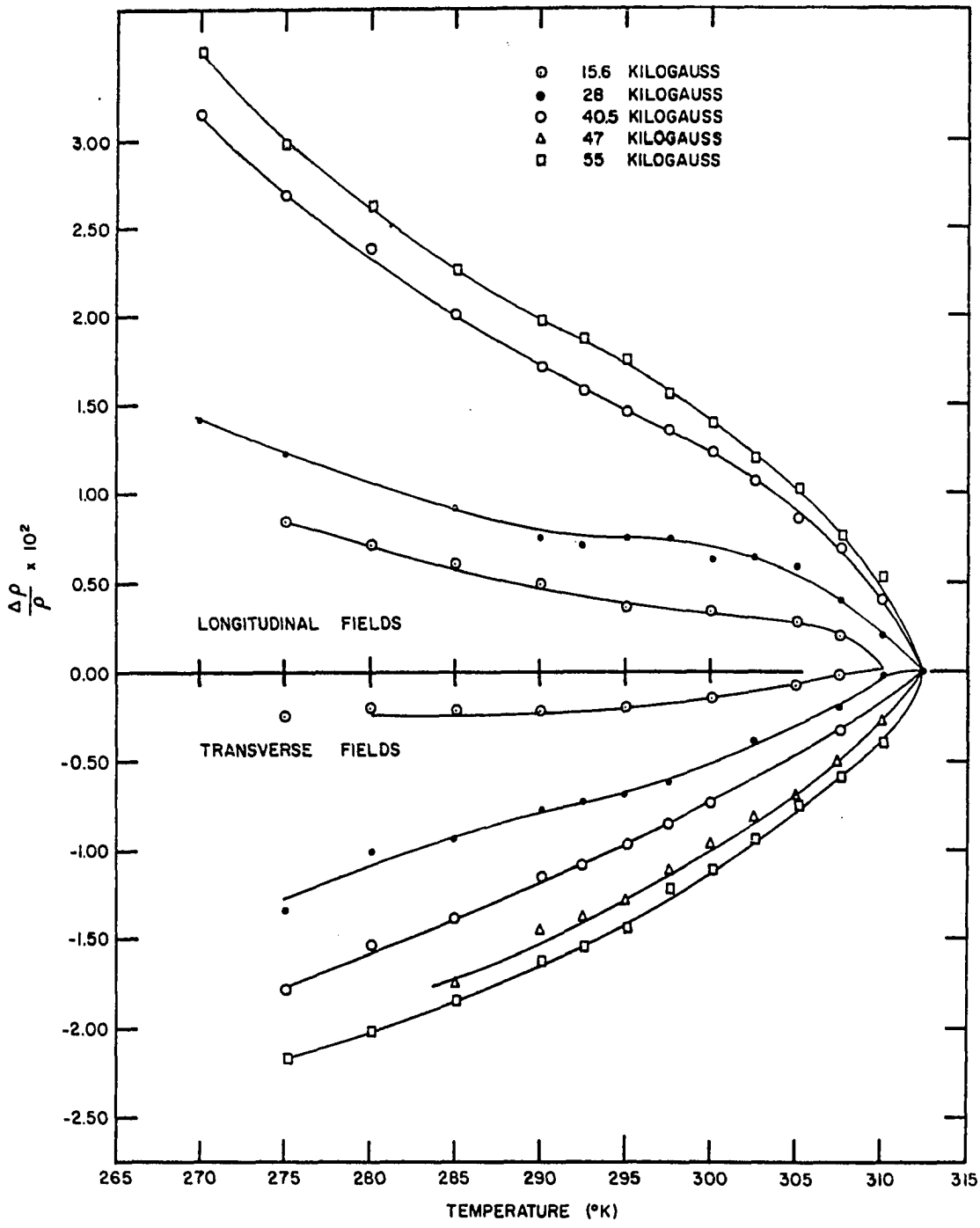

Figure 26. Isofield curves of $[\rho(H_c) - \rho(0)]/\rho(H_c)$ versus temperature for a field cooled single crystal of chromium

The field cooling magnetoresistance curves were obtained by subtracting the curve $\rho(H_c)$ from the curve $\rho(H_c = 0)$ and dividing by $\rho(H_c = 0)$.

Isotherms are shown in Figure 27. These curves were plotted directly from the field cooling magnetoresistance curves.

It should be emphasized that the normal magnetoresistance was found to be negligible at these temperatures. At 300°K no change was observed upon turning the field up to 55 kilogauss even though a change of 0.04% could be detected. It was also found that after the crystal had been cooled in a magnetic field the crystal retained its anisotropy until it had been warmed above the Néel temperature.

Neutron Diffraction Results

In cooperation with H. Bjerrum Møller of the Danish A.E.C., the magnetic scattering of 4Å neutrons from single crystals of chromium alloys with vanadium (1.5%, 2.0%), manganese (1.76%, 2.16%), and rhenium (0.07%, 0.09%, 0.19%, 0.78%) has been studied at room temperature and at 95°K. A crystal spectrometer situated at the DR3 reactor of the Danish Atomic Energy Commission, Research Establishment Riso was used for these measurements. Conventional rocking curves

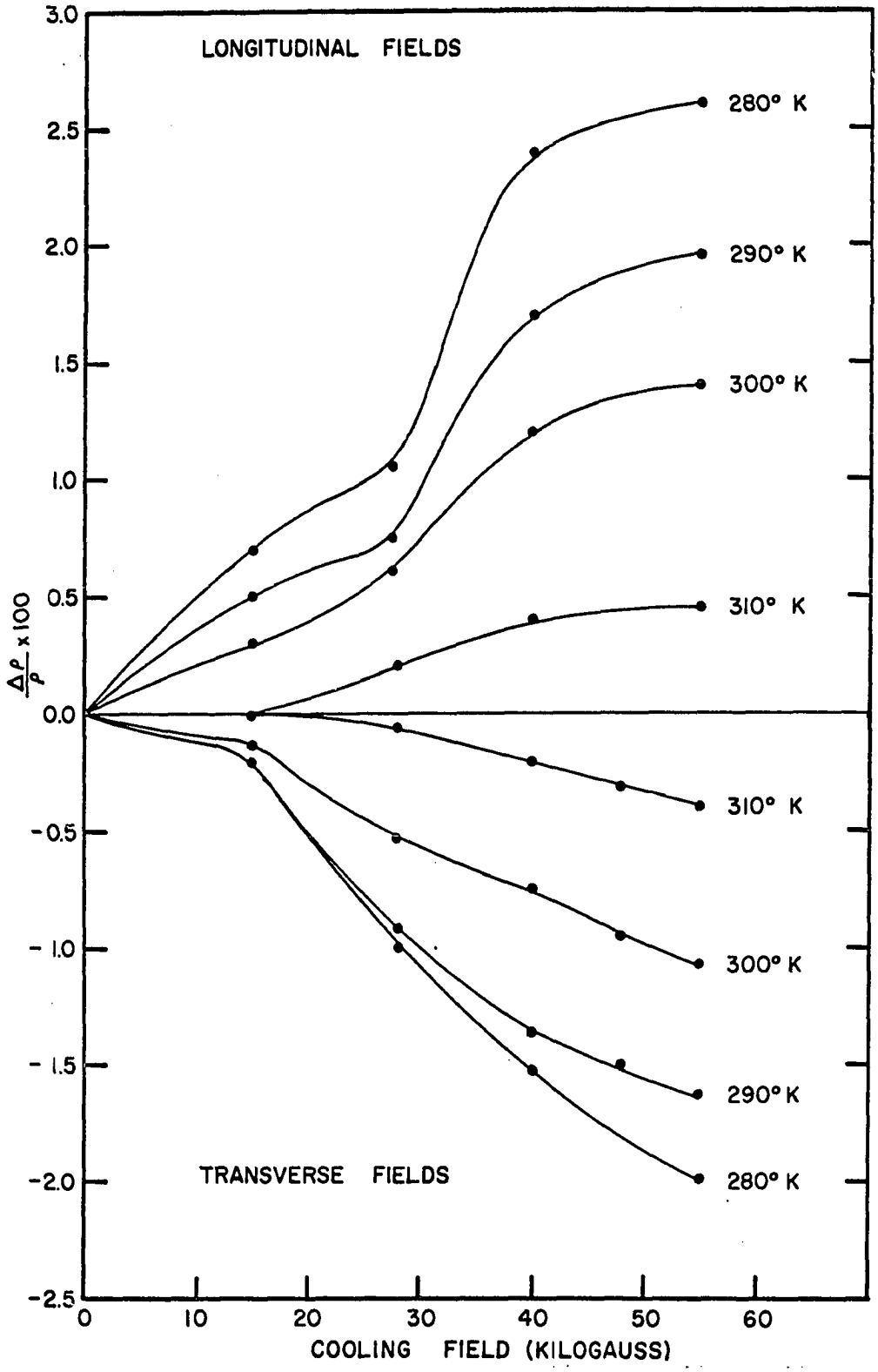

Figure 27. Isothermal curves of $[\rho(H_c) - \rho(0)]/\rho(H_c)$ versus cooling field for a single crystal of pure chromium

and 2:1 scans were made near (100) in an (001) plane on single crystal samples approximately 1 cm in diameter and several cms in length.

The results for a 2.0%V single crystal are shown in Figure 28. The two vertical lines correspond to the position of the satellite peaks for pure chromium. Thus, the addition of vanadium has caused a larger separation of the satellite peaks than for pure chromium. The corresponding repeat distance, $1/\delta$, of the magnetization wave is calculated to be 15.1 lattice constants for this alloy. The intensities of the satellite peaks have decreased by an order of magnitude from those found for pure Cr. This means that the amplitude of the magnetization waves and, therefore the magnitude of the energy gaps, have decreased by an order of magnitude from those found in pure Cr. The central peak which occurs is due to second order neutrons. Similar results were found for a 1.5%V single crystal and are listed in Table 3. We can therefore conclude from the neutron diffraction results for the chromium-vanadium alloys that the magnitude of the energy gaps is rapidly reduced by the addition of V while the positions of the superzone planes are shifted farther from the (1/2,0,0) type points in reciprocal space.

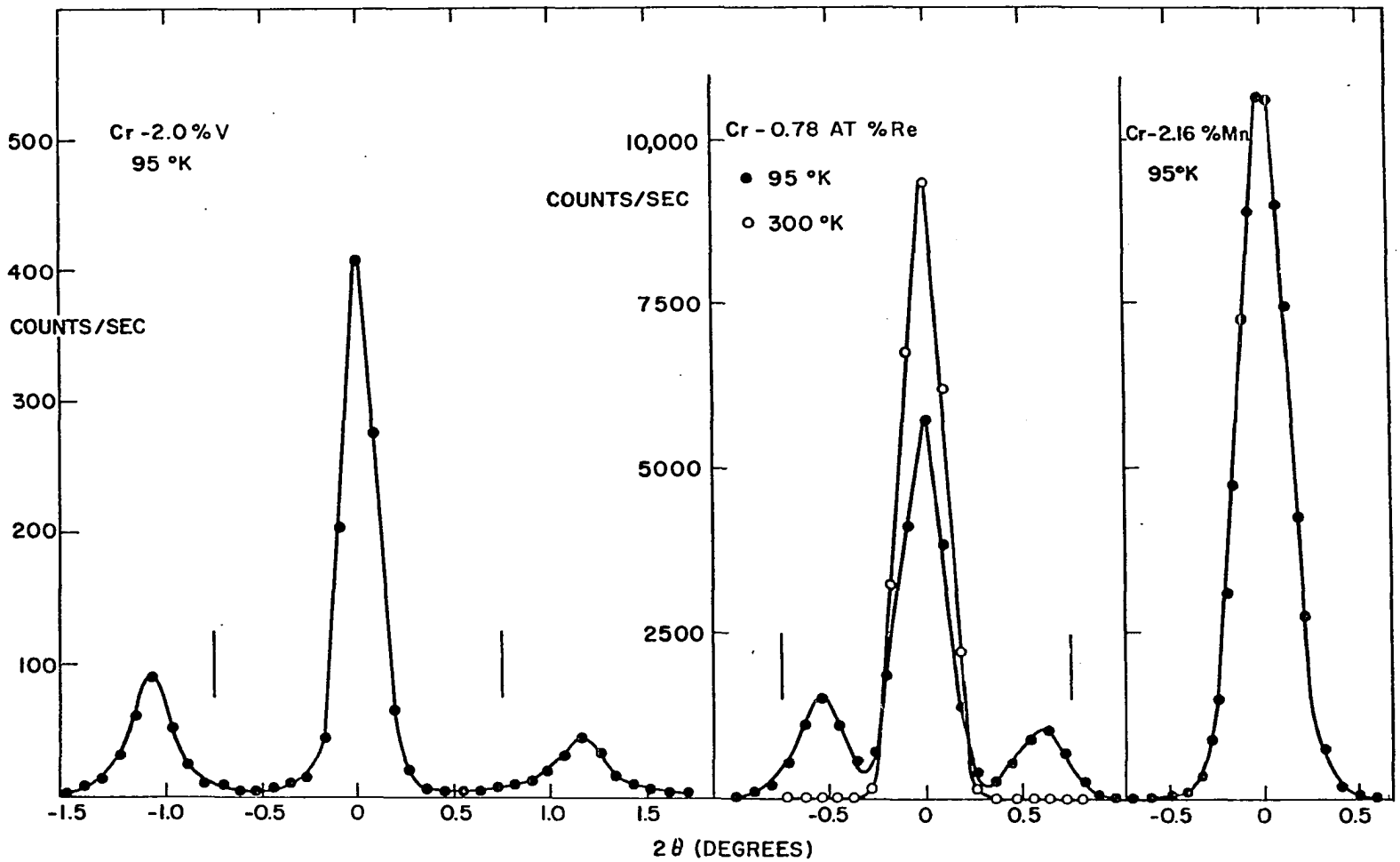

Figure 28. Neutron diffraction 2:1 scans in dilute chromium alloys at 4Å (the vertical lines indicate the satellite positions for pure Cr at 95°K)

Table 3. Intensities of neutron diffraction peaks for chromium alloys[a]

Alloy Concentration (Atomic percent)	δ^{-1}	Peak intensity (counts/sec) (200)	(100)	(1-δ, 0, 0)
Pure Cr	26.0, 20.8*(L)	25000	680(second order)	550
1.5%V	14.7*	48000	1100* "	800*
2.0%V	15.1*	23000	410* "	90*
0.07%Re	27.0, 21.0*(L)	35000	1500 "	1000
0.09%Re	29.0	37000	1500 "	1400
0.19%Re	31.2, 22.5*(L)	22000	1500 "	700
0.78%Re	∞,∞,28.5*	44000	9000,6000*	1500*
1.76%Mn	∞	19000	8000,11000*	
2.16%Mn	∞	19000	9000	

[a]The values marked with an asterisk were determined at 95°K, the others at 300°K; (L) indicates that magnetization waves are longitudinally polarized.

The results for a 1.76%Mn single crystal are shown in Figure 28. No satellite peaks are observed for this crystal or for a 2.16%Mn crystal (Table 3). All the satellite peaks have thus coalesced into a large single peak at (100) and the

magnetization waves have become commensurate with the lattice. The magnetic structure for these alloys is then a simple antiferromagnetic structure. From the intensity of the peak it can be seen that magnetic moment is larger than it is in pure chromium. In this case the contribution of second order neutrons is only about 5% of the total intensity. Thus the neutron diffraction results for chromium-manganese alloys imply that the magnitude of the energy gap is increased by the addition of Mn and that, after a sufficient amount of manganese has been added, the positions of the energy gap are at the planes $k_x = \pi/a$, etc.

The results for a 0.78%Re single crystal are shown in Figure 28. At room temperature no satellite peaks are observed and the magnetization wave is commensurate with the lattice. At 95°K, however, both commensurate and incommensurate components are observed. Samples containing less rhenium (Table 3) were found to have magnetization waves which were incommensurate with the lattice but with smaller satellite separation than found in pure chromium. The addition of rhenium also causes an increase in the satellite intensities although some difficulties were encountered in interpreting the intensities of the peaks due probably to

residual strains in the sample. Similar difficulties have been reported by Møller *et al.* (39). The addition of rhenium to chromium, therefore, causes the magnitude of the energy gap to increase while the position of the superzone planes shifts towards the (1/2,0,0) point in reciprocal space and eventually occurs at the (1/2,0,0) point for high enough electron concentration.

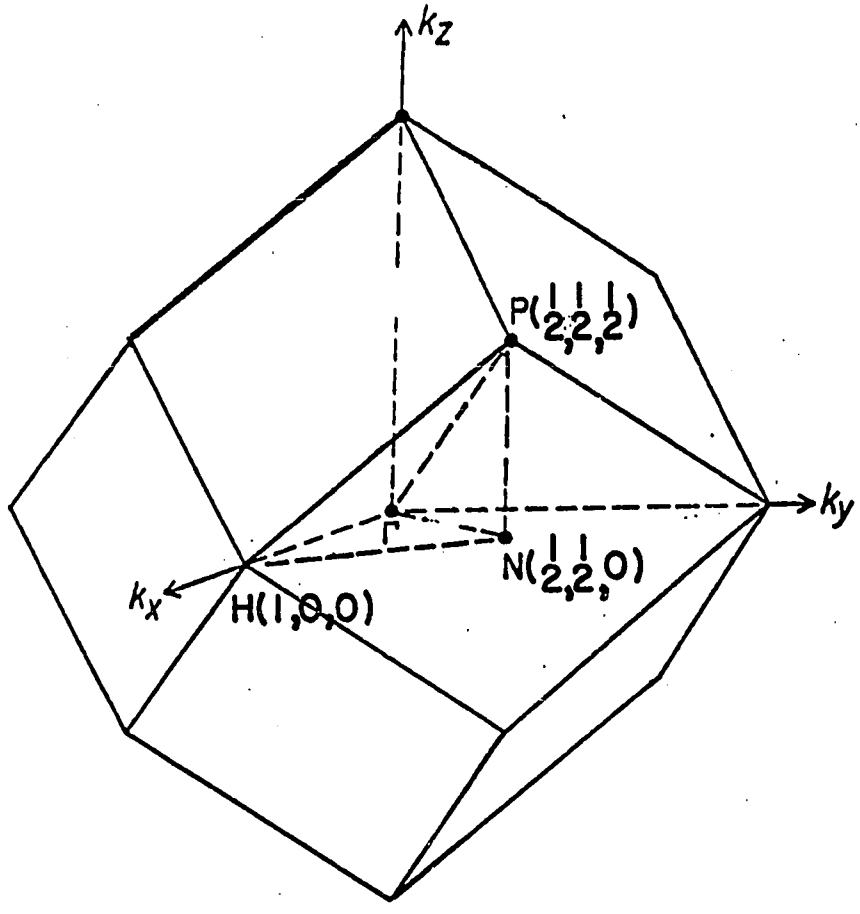

Figure 29. Brillouin zone for a body centered cubic lattice

Figure 30. Intersection of chromium Fermi surface with 1/48th zone faces (The lined areas represent regions occupied by electrons and the dotted areas represent regions occupied by holes; the positions of the points Γ, H, P, N are given in Figure 29; Q/2 gives the position of the superzone plane for pure Cr at room temperature)

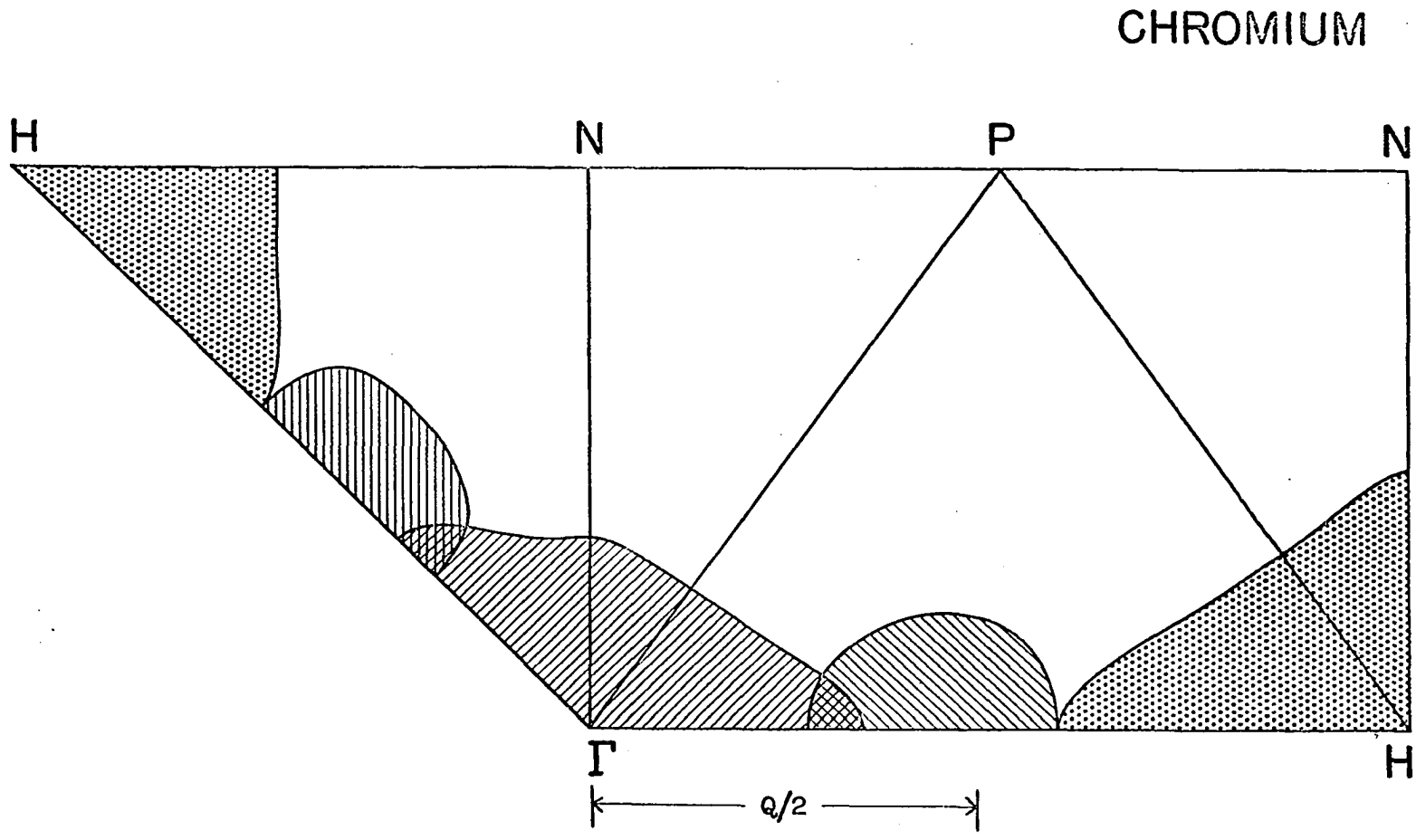
CHROMIUM
H
N
P
N
Γ
H
Q/2

DISCUSSION OF RESULTS

Chromium Alloys

The magnetic structures deduced from the neutron diffraction measurements give qualitative support to the theory of Tachiki and Nagamiya (50). As predicted by the theory, increasing the electron concentration by the addition of Re or Mn to Cr causes the oscillatory magnetization waves to become more nearly commensurate with the lattice until finally, above a certain electron concentration, the periodicity of the magnetization waves actually becomes commensurate with the lattice periodicity. Decreasing the electron concentration by the addition of V causes the period of the magnetization waves to become less commensurate with the lattice period, also in agreement with the theory. The amplitudes of the magnetization waves were found to decrease with the addition of V and to increase with the addition of Mn or Re to Cr. Such behavior is also in qualitative agreement with the theory. The higher curves in Figure 1 allow a larger value of $\bar{g}$ as the solution to Equation 8 and the amplitude of the magnetization wave is therefore expected to increase as the electron concentration is increased. These

neutron diffraction results are in agreement with those of Hamaguchi et al. (26) on powdered samples.

For a cubic metal, the results of Miwa (38) and Elliott and Wedgwood (19) show that the electrical resistivity is of the form

$$\rho = \rho(0)\ (1+\alpha), \tag{42}$$

where $\rho(0)$ includes the effects of magnetic scattering. The neutron diffraction results show that the moment in the Cr-V alloys is small, however, so that the magnetic scattering should also be small. The experimentally determined values of α (Figure 14) are therefore assumed to be determined primarily by the magnitudes and positions of the energy gaps in the Fermi surface. This is not the case for the thermoelectric power, however, because the anomalies have much larger magnitudes than the resistivity anomalies. From Equation 28 this probably implies a rather large energy dependence of the electron scattering. In this case it is difficult to separate the effect of the distortion of the Fermi surface from the magnetic disorder scattering.

The most striking feature of the transport properties is the persistence of large anomalies as the V concentration

is increased. This is particularly surprising because the neutron diffraction results show that the addition of V greatly reduces the magnitude of the moment and, therefore, of the energy gap. Hence, from Equation 15 one expects the parameter α, and therefore the magnitude of the anomalies, to decrease very rapidly with increasing V concentration. The resistivity must therefore be more sensitive to the position of the superzone gaps than to their magnitudes in this case. From Equation 16 this is taken to imply that the superzone planes touch a large piece of the Fermi surface.

The Brillouin zone for chromium is shown in Figure 29 and a cross-section of the Fermi surface as calculated recently by Loucks (34) is shown in Figure 30. The feature of particular interest is the electron surface centered on Γ which has a very flat face normal to [100]. If we assume that the face of the electron surface intersects the [100] axis at approximately (0.48,0,0) for pure Cr, then a very consistent explanation of both the magnetic and transport properties can be given for the alloys. In analogy with the theory of Tachiki and Nagamiya it is suggested that the period of the oscillatory magnetization is determined by the position of the flat face of the electron surface. Thus as

V is added, the position of the flat face moves towards Γ while the corresponding wave vector of the oscillatory magnetization wave decreases in magnitude. When Mn or Re is added the flat face moves towards H and the magnitude of the wave vector increases until, above a certain electron concentration, it becomes equal to $2\pi/a$. Thus the superzone planes are always touching the electron surface and can therefore lead to the observed behavior of the transport properties.

According to the band structure calculation the flat face intersects the [100] axis just beyond the (1/2,0,0) position while the superzone plane of interest intersects at $(1/2)(1-\delta,0,0)$. The discrepancy in position may not be important, however, because the band structure calculation has not been tested by a direct Fermi surface experiment. Furthermore the band structure calculation neglects the intra-atomic exchange term which is an important feature of the theory of Tachiki and Nagamiya (50).

If the conclusions reached above are correct, a measurement of the magnitudes of the q vectors of the magnetization waves determines a dimension of the Fermi surface. Because of the low purity of the materials involved such a determina-

tion would be very difficult with the usual techniques.

Møller et al. (39) have reported a large amount of short range order which persists to unusually high temperatures above the Néel temperature for pure Cr. Both the thermoelectric power and the electrical resistivity of Cr show a large departure from linearity in this region. Similar behavior was found for the Cr-Re and Cr-Mn alloys which may be due to the effects of short range order. For Cr-V alloys, however, the resistivity and thermoelectric power rapidly become linear above the Néel temperature suggesting that the amount of short range order has been greatly reduced. The effect could be due, however, to the reduced moment of these alloys. A measurement of the critical scattering of neutrons from the alloys could be used to determine the amount of short range order present and thus possibly explain the observed behavior. The non-linearity of the transport properties above the Néel temperature for the Cr-Re and Cr-Mn alloys makes the data very difficult to analyze.

Increased phonon scattering causes the phonon drag contribution to be diminished by the addition of impurities (46). However, for the Cr-Mn alloys a large maximum in the thermoelectric power appears at about 60°K. Furthermore the

size of this maximum is much larger for a sample containing 0.96%Mn than for a sample containing 0.35%Mn. According to the neutron diffraction results of Hamaguchi et al. (26) the 0.96%Mn sample is a simple antiferromagnetic whereas the 0.35%Mn sample has an incommensurate magnetic structure. This fact, together with the fact that the Mn alloys have a larger moment than pure Cr, suggests that magnon drag makes an important contribution to the thermoelectric power for these alloys. It would be of interest to see whether or not the Cr-Re alloys have a similar behavior.

Discussion of Field Cooling Results

Results obtained by Montalvo and Marcus (40) and by Watts (54) on the bulk magnetization of pure Cr have shown that a single crystal of Cr, which has been cooled through its Néel temperature in a magnetic field, can exhibit tetragonal symmetry. Møller et al. (39) studied the magnetic scattering of neutrons from Cr and found that the magnetic structure of a strained crystal does not have cubic symmetry. They found that the intensities of the satellites at $(1\pm\delta,0,0)$ were greater than the intensities of the satellites at $(0,1\pm\delta,0)$. These results suggest that there is an

anisotropy of the amplitudes of the magnetization waves.

Anisotropy of the transport properties of strained or field cooled specimens is therefore expected. For a tetragonal axis in the z direction, the calculations of Miwa (38) and Elliott and Wedgwood (19) show that the non-zero components of the electrical resistivity are of the form

$$\rho_{zz} = \rho_{zz}(0)\ (1+\alpha_z) \tag{43}$$

$$\rho_{xx} = \rho_{yy} = \rho_{xx}(0)\ (1+\alpha_x) \tag{44}$$

where $\rho_{zz}(0)$ and $\rho_{xx}(0)$ are essentially equal and include the effects of impurity scattering, phonon scattering, and magnetic disorder scattering. The resistivity is now a function of direction because the parameter α, which is proportional to the magnitude of the energy gap, is a function of direction. From Figure 25 we see that the electrical resistivity for a single crystal of pure Cr cooled through its Néel temperature in a magnetic field actually exhibits this behavior.

Since the resistivity is greater for the direction parallel to H_c than for the direction perpendicular to H_c we conclude that the energy gap associated with the direction parallel to H_c is larger than the energy gaps associated with

directions perpendicular to H_c. This implies that the amplitude of the magnetization wave which propagates along an axis parallel to H_c is greater than the amplitudes of the magnetization waves which propagate along directions perpendicular to H_c. Thus, it appears that the effect of field cooling a single crystal of pure Cr is to enhance the amplitudes of the magnetization waves which propagate parallel to H_c and to diminish the amplitudes of those propagating perpendicular to H_c. It has been assumed, of course, in the above discussion that H_c is always parallel to one of the cube axes since this was the experimental configuration. These conditions were chosen because the magnetization waves propagate along the cube axes and the superzone planes are perpendicular to the [100] directions in reciprocal space.

Implicit in the above discussion has been the assumption that the normal magnetic structure of a single crystal of Cr consists of magnetic domains each of which has cubic symmetry, or is in fact a single domain. This corresponds to Model II discussed in Chapter II. If, however, Model I were correct and each small magnetic domain had tetragonal symmetry, then the present experimental results could be explained by assuming that the field cooling produces an

unbalanced domain distribution.

Model I is thought to be incorrect, however, because of several recent developments. Weiss (55) has deduced from the thermal expansion data of Bolef and De Klerk (8) that Model I would imply a broadening of the X-ray Bragg peak by a factor of about 40 as a sample of chromium is cooled through its Néel temperature. The experimental results of Weiss (55) show no such broadening and he concludes that his results are consistent with Model II. Recent studies of the De Haas-Van Alphen effect by Marcus[1] have shown that all the frequencies which have been observed thus far are shifted by the application of a cooling field. This is fairly conclusive evidence for the validity of Model II because Model I requires that no shift in the frequencies can occur for field cooled specimens; only a change in amplitudes is possible.

From Figure 26, which shows the change in resistance for different cooling fields, it can be deduced on the basis of Model I that the amount of unbalance in the domain distribution would depend on the magnitude of H_c. From Figure 27 it is seen that the effect is not saturated for a cooling field

---

[1]Marcus, J. A., Evanston, Illinois. De Haas-Van Alphen effect in Cr. Private communication. 1965.

of 55 kilogauss and that much higher cooling fields would be required for saturation. A study of the De Haas-Van Alphen effect by Watts (54), however, has shown that for H_c = 65 kilogauss the field cooled specimens exhibit complete tetragonal symmetry, in the sense that none of the De Haas-Van Alphen frequencies for H parallel to the field cooling direction [001] coincides with any frequencies for H parallel to [010] or [100]. Thus for Model I his results imply saturation of the effect. This does not seem to be consistent with the present results.

SUMMARY AND SUGGESTIONS FOR FUTURE WORK

Summary

The experimental results which have been reported in this dissertation have led to some conclusions regarding the nature of the antiferromagnetic state of pure Cr and its alloys and have given some information about the electronic structure and the scattering mechanisms in these metals. The lack of quantitative theories hinders the interpretation of the data but through the use of qualitative arguments the results can be at least partially understood and some interesting properties of these alloys revealed.

From the neutron diffraction results some definite conclusions about the antiferromagnetic structure of dilute Cr alloys can be reached. In particular, the effect of alloying V, Mn and Re with Cr on the relative magnitudes of the energy gaps and on the positions of the superzone planes can be determined. This information is of the utmost importance for interpreting the transport property measurements. Excellent qualitative agreement is found between the neutron diffraction results and the theory of Tachiki and Nagamiya (50). Of particular interest is the verification of their prediction

that, above a certain electron concentration, the period of the oscillatory magnetization waves becomes commensurate with the period of the lattice. It appears that the basic elements of their theory are correct and that it gives a satisfactory explanation for the type of antiferromagnetism which is found in Cr. Better tests of their theory will be possible when the calculation is extended to a more realistic model of the Fermi surface.

Very striking anomalies in the transport properties of these alloys are found just below their Néel temperatures. The presence of the anomalies can be understood from the appearance of the superzone energy gaps together with the rapid variation of magnetic disorder scattering. The persistence of large anomalies as V is added to Cr is explained by assuming that the superzone planes are touching a large portion of the Fermi surface. Both the transport and magnetic properties of the alloys are consistent with this assumption and it is suggested that this may, in fact, be a way to determine a dimension of the Fermi surface for these alloys. It is also suggested that the discrepancy between the existing band structure calculation (34) and the band structure required for the above assumption to be valid may

be due to neglect of the intra-atomic exchange term which appears to be an important factor in determining the antiferromagnetic properties.

An extremely interesting effect was discovered in the electrical resistivity of field cooled single crystals of chromium. It was found that, as a result of the tetragonal symmetry which is induced in the oscillatory magnetization waves, the electrical resistivity becomes anisotropic and the effect is sufficiently large that it can easily be observed and studied. These measurements give conclusive evidence that the amplitude of the magnetization wave which is propagating parallel to the cooling field is enhanced while the amplitudes of the waves propagating along the other two cube axes are diminished.

Suggestions for Future Work

Although numerous measurements of the electrical resistivity of dilute alloys of Cr have been reported, no systematic study of the magnitude of the anomaly has been made. Previously, only polycrystalline samples have been used. The present study has shown, however, that valuable information can be obtained by making neutron diffraction and transport property measurements on single crystal specimens.

This study should be extended to other dilute alloys of Cr. In particular, alloying Cr with W and Mo should be interesting because of their similar band structures (34). A study of these alloys should give some insight into the reason why Cr is the only member of this group which exhibits antiferromagnetism.

It is of interest to study the transport properties of the Re and Mn alloys further in order to observe the behavior as the magnetization waves become commensurate with the lattice. It would appear that, since the Fermi surface should expand until the superzone plane actually intersects the surface rather than just touching it, the magnitude of the anomaly might suddenly decrease. The magnetic scattering will be greatly increased for these alloys, however, so that the contribution from the superzone planes will be difficult to isolate.

The field cooling effect may be of potential use for studying the various electron scattering mechanisms individually. The difficulty in interpreting the electrical resistivity or thermoelectric power of pure Cr is in separating three magnetic effects:

(1) the magnetic disorder scattering

(2) the effect of the magnitude of the energy gap

(3) the effect of the position of the energy gap.

All of these effects are temperature dependent. The electrical resistivity of field cooled specimens, however, can be studied at a fixed temperature. In particular at very low temperatures where there is no magnetic disorder scattering, the effect on the resistivity of changing the magnitude of the energy gap can be studied separately. A study of the thermoelectric power of field cooled specimens may also allow a separation of the effects involved and could lead to a better understanding of the mechanisms which influence the thermoelectric power of such magnetic materials. These studies, in combination with neutron diffraction measurements on field cooled specimens, should lead to a much better understanding of the antiferromagnetism of Cr and should be of potential value in interpreting the results of Fermi surface studies. An understanding of the mechanism which produces the tetragonal symmetry in the magnetic structure of field cooled crystals might also be provided.

It would be of interest to see whether or not the electrical resistivity of field cooled specimens of Cr alloys shows the same behavior as found for pure Cr. For Cr-V alloys, where the antiferromagnetic state is less stable than

for pure Cr, a rather large effect might be predicted whereas a smaller effect might be predicted for the Cr-Re and Cr-Mn alloys.

The observation of a magnon drag contribution to the low temperature thermoelectric power of Cr-Mn alloys leads one to expect a similar contribution for the Cr-Re alloys. Magnon drag has received very little attention and it is possible that these Cr alloys could provide a very suitable system to study the effect.

It is obvious that much work is needed in order to obtain a complete understanding of the basic properties of chromium and its alloys. The Fermi surface must be accurately determined before quantitative explanations of the magnetic and transport properties can be given. Previously, such a determination has been very difficult because of the extra complications which arise from the magnetic structure. It is hoped that the present results, together with those further studies which have been suggested, can lead to an understanding of the relationship between the magnetic structure and the electronic structure. It may then be possible to understand the results of experiments which give explicit information about the Fermi surface, such as the galvanomagnetic and De Haas-Van Alphen effects.

LITERATURE CITED

1. Arajs, S., R. V. Colvin, and M. J. Marcinkowski, J. Less-Common Metals 4, 46 (1962).

2. Asdente, M. and J. Friedel, Phys. Rev. 124, 384 (1961).

3. Bacon, G. E., Acta Cryst. 14, 823 (1961).

4. Bailyn, M., Phys. Rev. 126, 2040 (1962).

5. Barnes, R. G. and T. P. Graham, Phys. Rev. Letters 8, 248 (1962).

6. Bardeen, J., L. N. Cooper, and J. R. Schrieffer, Phys. Rev. 108, 1175 (1957).

7. Beaumont, R. H., H. Chihara, and J. A. Morrison, Phil. Mag. 5, 188 (1960).

8. Bolef, D. I. and J. De Klerk, Phys. Rev. 129, 1063 (1963).

9. Booth, J. G., Effect of electron concentration on the properties of alloys and metals. Battelle Memorial Institute annual topical report on contract No. Nonr-3589-(00) to Office of Naval Research, Department of the Navy. 1964.

10. Borelius, G. W., H. Keesom, C. H. Johansson, and J. O. Linde, Proc. K. Akad. Amst. 35, 10 (1932).

11. Born, H. J., S. Legvold, and F. H. Spedding, J. Appl. Phys. 32, 2543 (1961).

12. Butylenko, A. K. and V. N. Gridnyev, Ukrayin. Fiz. Zh. 9, 325 (1964).

13. Bykov, V. N., V. S. Galovkin, N. V. Ageef, V. A. Levdik, and S. I. Vinogradov, Soviet Phys. Doklady 4, 1070 (1960).

14. Carlson, O. N., F. A. Schmidt, and W. M. Paulson, Trans. Quar. Am. Soc. Metals 57, 356 (1964).

15. Christian, J. W., J. P. Jan, W. B. Pearson, and I. M. Templeton, Proc. Roy. Soc. (London), A245, 213 (1958).

16. Collings, E. W., F. T. Hedgcock, and A. Siddiqui, Phil. Mag. 6, 155 (1961).

17. Corliss, L., J. Hastings, and R. Weiss, Phys. Rev. Letters 3, 211 (1959).

18. Edwards, A. R., Phil. Mag. 8, 311 (1963).

19. Elliott, R. J. and F. A. Wedgwood, Proc. Phys. Soc. 81, 84b (1963).

20. Fine, M. E., E. S. Greiner, and W. C. Ellis, Trans. AIME 189, 56 (1951).

21. Finnemore, D. K., J. E. Ostenson, and T. F. Stromberg, U.S. Atomic Energy Commission Report IS-1046 [Iowa State Univ. of Science and Technology, Ames. Inst. for Atomic Research]. 1964.

22. Gennes, P. G. De and J. Friedel, J. Phys. Chem. Solids 4, 71 (1958).

23. Gold, A. V., D. K. C. MacDonald, W. B. Pearson, and I. M. Templeton, Phil. Mag. 5, 765 (1960).

24. Gurevich, L. E. and G. M. Nedlin, Societ Physics-JETP 18, 396 (1964).

25. Hamaguchi, Y. and N. Kunitomi, J. Phys. Soc. Japan 19, 1849 (1964).

26. Hamaguchi, Y., E. O. Wollan, and W. C. Koehler, Neutron diffraction investigation of chromium with small additions of manganese and vanadium. [to be published in Phys. Rev. ca. 1965].

27. Hansen, M., Constitution of binary alloys, 2nd ed., New York, N.Y., McGraw-Hill Book Co., Inc. 1958.

28. Huebener, R. P., Phys. Rev. A135, 1281 (1964).

29. Kasuya, T., Prog. Theor. Phys. (Kyoto) 16, 58 (1956).

30. Kasuya, T., Prog. Theor. Phys. (Kyoto) 22, 227 (1959).

31. Lidiard, A. B., Proc. Phys. Soc. A66, 1188 (1953).

32. Lomer, W. M., Proc. Phys. Soc. 80, 489 (1962).

33. Lomer, W. M. and J. A. Marcus, Magnetic anisotropy and hysteresis in chromium. [to be published in the Proceedings of the International Conference on Magnetism, Nottingham, September 1964. ca. 1965].

34. Loucks, T. L., APW Fermi surfaces in chromium, molybdenum and tungsten, [to be published in Phys. Rev. ca. 1965].

35. MacDonald, D. K. C., Thermoelectricity: An introduction to the principles, New York, John Wiley and Sons, Inc. 1962.

36. Mackintosh, A. R. and L. R. Sill, J. Phys. Chem. Solids 24, 501 (1963).

37. Marcinkowski, M. J. and H. A. Lipsitt, J. Appl. Phys. 32, 1238 (1961).

38. Miwa, H., Prog. Theor. Phys. (Kyoto) 28, 208 (1962).

39. Møller, H. Bjerrum, K. Blinowski, A. R. Mackintosh, and T. Brun, Solid State Communications 2, 109 (1964).

40. Montalvo, R. A. and J. A. Marcus, Phys. Letters 8, 151 (1964).

41. Morton, M. E. De, Nature 181, 477 (1958).

42. Mott, N. F. and H. Jones, The theory of the properties of metals and alloys, New York, N.Y., Dover Publications, Inc. 1958.

43. Overhauser, A. W., Phys. Rev. 128, 1437 (1962).

44. Powell, R. L., M. D. Bunch, and R. J. Corruccini, Cryogenics 1, 139 (1961).

45. Pursey, H., J. Inst. Metals 86, 362 (1958).

46. Schroeder, P. A., R. Wolf, and J. A. Woollam, Phys. Rev. 138, A105 (1965).

47. Shirane, G. and W. J. Takei, J. Phys. Soc. Japan 17, Suppl. B-3, 35 (1962).

48. Sill, L. R., Seebeck effect in heavy rare earth single crystals. Unpublished Ph.D. thesis. Ames, Iowa, Library, Iowa State University of Science and Technology. 1964.

49. Shull, C. G. and M. K. Wilkinson, Rev. Mod. Phys. 25, 100 (1953).

50. Tachiki, M. and T. Nagamiya, Phys. Letters 3, 214 (1963).

51. Taylor, M. A., J. Less-Common Metals 4, 476 (1962).

52. Vries, G. De, J. Phys. et Rad. 20, 438 (1959).

53. Vries, G. De and G. W. Rathenau, J. Phys. Chem. Solids 2, 339 (1957).

54. Watts, B. R., Phys. Letters 10, 275 (1964).

55. Weiss, R. J., Phys. Letters 10, 45 (1964).

56. Wilkinson, M. K., E. O. Wollan, W. C. Koehler, and J. W. Cable, Phys. Rev. 127, 2080 (1962).

57. Wilson, A. H., The theory of metals, 2nd ed., London, England, Cambridge University Press. 1958.

58. Yosida, K., Prog. Theor. Phys. (Kyoto) 28, 759 (1962).

59. Ziman, J. M., Electrons and phonons, London, England, Oxford University Press. 1960.

ACKNOWLEDGMENTS

I wish to thank my major professor, Dr. A. R. Mackintosh, for suggesting this problem and for many valuable discussions throughout the course of this investigation.

I wish to thank Professor R. C. Young for his advice and encouragement and for his cooperation in the use of the magnets.

Especial acknowledgment is due Dr. F. A. Schmidt for supplying the single crystals of chromium alloys without which these experiments would not have been possible.

I wish to thank Dr. H. Bjerrum Møller for performing the neutron diffraction measurements.

Acknowledgment is given to Mr. D. R. Stone, Mr. T. O. Brun, Mr. J. Milliken, and Dr. R. J. Kearney for assembling and maintaining the superconducting magnet system.

Thanks are due Dr. L. E. Spanel, Dr. P. N. Dheer, and Mr. L. D. Muhlestein for many discussions concerning the experimental apparatus.

I wish to acknowledge the extremely competent assistance of Mr. B. A. Haskell, Mr. A. A. Matthews and Mr. D. Grotzky with the sample preparation.

I wish to thank the Department of Health, Education and

Welfare and the IBM Corporation for fellowships during my graduate study.

Grateful acknowledgment is given to my wife, Bessie, for her patience and understanding throughout my graduate study and for her typing of the rough draft of this manuscript.